P-34

NASA Technical Paper 3014

September 1990

Graphite/Epoxy Composite Adapters for the Space Shuttle/Centaur Vehicle

Harold J. Kasper
and Darryl S. Ring

Date for general release August 1992

NASA

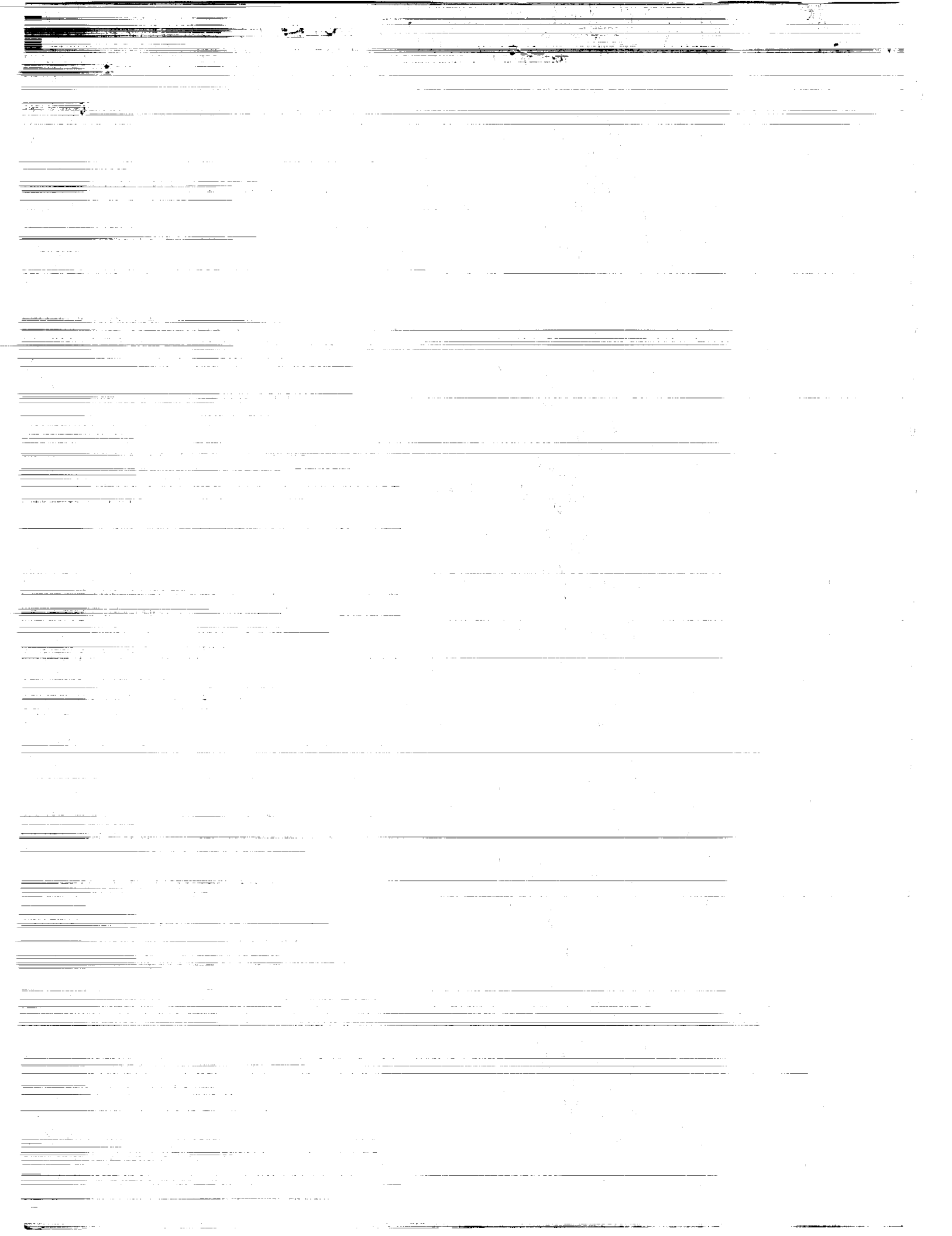

NASA Technical Paper 3014

1990

Graphite/Epoxy Composite Adapters for the Space Shuttle/Centaur Vehicle

Harold J. Kasper
Lewis Research Center
Cleveland, Ohio

Darryl S. Ring
General Dynamics Space Systems Division
San Diego, California

NASA
National Aeronautics and Space Administration
Office of Management
Scientific and Technical Information Division

Summary

Launching various NASA scientific and Air Force spacecraft from the space shuttle requires a high-energy upper stage capable of being deployed from the cargo bay. Two redesigned versions of the Centaur vehicle which used a graphite/epoxy composite material for the forward and aft adapters were selected. Since this was the first time a graphite/epoxy material was used for Centaur major structural components, the development of the adapters was a major effort. Although the shuttle/Centaur program was terminated in 1986, the results of this effort may be useful in future programs. This report includes (1) an overview of the composite adapter designs, (2) results of subcomponent design evaluation tests, and (3) composite adapter test results from a full-scale vehicle structural test.

Introduction

The decision to launch the Galileo and Ulysses spacecraft from the space shuttle created the need for a high-energy upper stage that could be deployed from the cargo bay. A redesigned Centaur vehicle which used hydrogen and oxygen propellants was selected for this purpose. Two vehicles designated as Centaur G-Prime were manufactured to accommodate the launch of each spacecraft individually. In addition, the Centaur G, which is a shortened version of G-Prime, was designed to accommodate various military missions and the NASA Magellan spacecraft. Because of certain design requirements, the decision was made early in the program to select a graphite/epoxy composite material for the aft adapter and the cylindrical portion of the forward adapter. This was the first time that a composite material was used for major structural components on the Centaur vehicle.

The shuttle/Centaur program was terminated in June 1986 following the Space Shuttle Challenger accident, thereby eliminating the opportunity for the shuttle/Centaur vehicles to fly. The G-Prime vehicles were in their final stages of preparation for launch when the program was terminated. Since the development of the composite adapters was a major effort, it seemed appropriate to document the results of this effort for possible beneficial use in future programs requiring composite adapters.

This summary report includes an overview of the composite adapter designs, results of subcomponent design evaluation tests, and composite adapter test results from a full-scale vehicle structural test.

Overview of Composite Adapter Designs

Shuttle/Centaur Vehicle Configurations

Centaur G-Prime vehicle.—The Centaur G-Prime shown in figure 1 was approximately 14 ft in diameter and 29.6 ft long. The main structural components were the forward adapter, liquid hydrogen (LH_2) tank, liquid oxygen (LO_2) tank, aft adapter, separation ring, and deployment adapter. The primary structural material was aluminum except for the LH_2 and LO_2 tanks, which were made of stainless steel. The forward adapter cylindrical section and the aft adapter were made of T300/934 graphite/epoxy composite.

Figure 2 shows the forward adapter with its aluminum skin/stringer conical section and its corrugated graphite/epoxy cylindrical section. The purpose of the corrugations was to allow for unrestricted contraction of the LH_2 tank interface ring (sta. 3591) with respect to the kick ring (sta. 3566) when the vehicle was loaded with cryogenic propellants. The cylindrical section consisted of six curved panels of equal circumferential length that were jointed together at their ends with graphite/epoxy splice plates and fasteners (fig. 3). The cylindrical structure was attached to the interface and kick rings by a bolted connection at each corrugation flat. Two cutouts were provided for pneumatic line penetrations (fig. 4). The basic laminate thickness was 0.040 in. with 0.196-in. buildup in the fastener locations.

The aft adapter shown in figure 5 was also T300/934 graphite/epoxy corrugated construction. It was approximately 120 in. in diameter and 11.2 in. long. The corrugated construction allowed for unrestricted contraction of the LO_2 tank interface ring (sta. 3759.22) with respect to the aft interface ring (sta. 3770.42) when the vehicle was loaded with cryogenic propellants. The aft adapter consisted of four curved panels that were joined by three graphite/epoxy splice plates (fig. 6). A 9.25-in. gap was left at the fourth joint to allow for the LH_2 tank fill-and-drain line penetration (fig. 7). Two cutouts were provided for the LO_2 tank vent line and instrumentation (fig. 8). The basic laminate thickness was 0.070 in. with 0.226-in. buildup in the fastener locations.

Centaur G vehicle.—Figure 9 shows the differences between the Centaur G-Prime and Centaur G vehicles. The G vehicle maintained the same principal structural components except that provision was made on the composite section of the forward adapter to mount an optional 22-hardpoint payload truss. Provision was also made at the forward end of the forward adapter cone frustrum to mount an optional eight-

hardpoint payload truss (not shown). Overall diameter of the G vehicle was the same as G-Prime, but the overall length was reduced from 30 ft to 20 ft.

The G vehicle forward adapter composite section was of the same construction and had the same diameter and length as the G-Prime vehicle composite section. The basic laminate thickness, though, was 0.060 in. with 0.216-in. maximum buildup thickness in the hardpoint and fastener locations. In addition, provision was made for two electrical packages to be beam mounted to the ends of the composite cylindrical

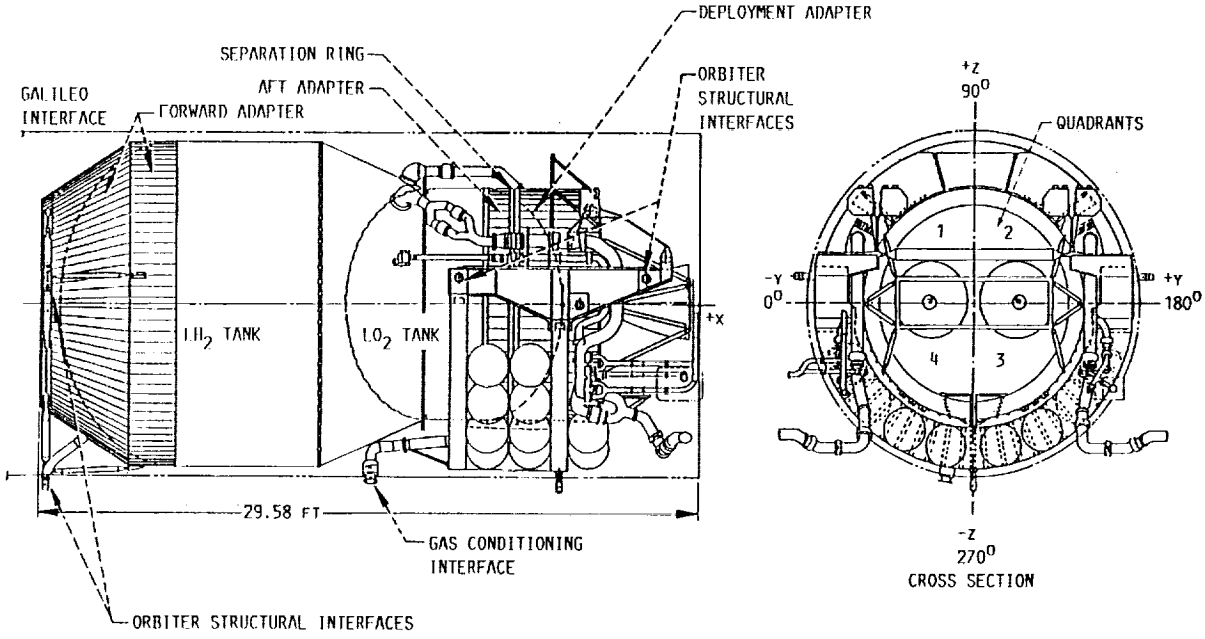

Figure 1.—G-Prime vehicle configuration and major structural interfaces.

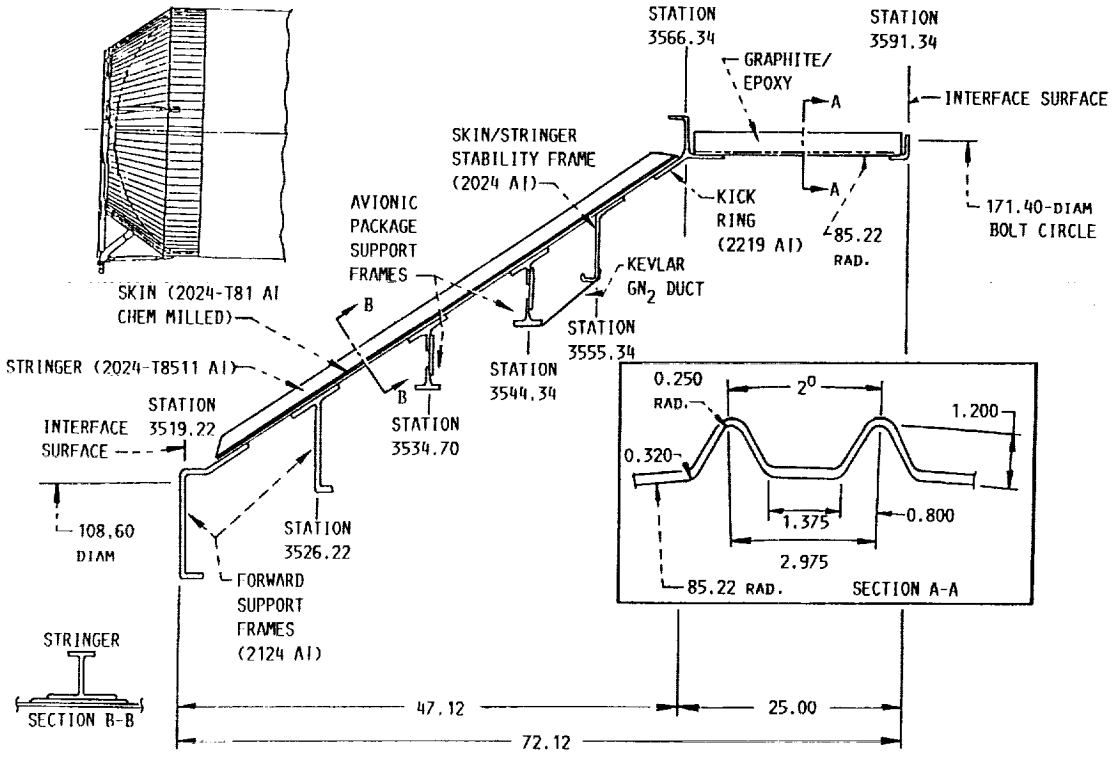

Figure 2.—G-Prime vehicle forward adapter section view (dimensions in inches unless noted otherwise).

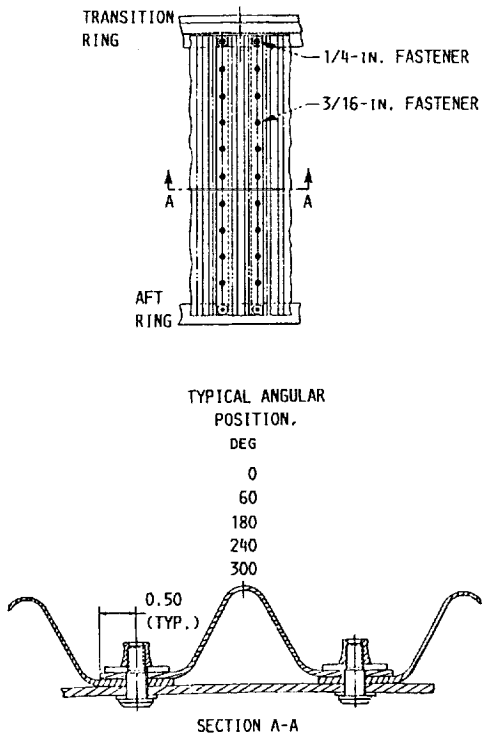

Figure 3.—Panel splice plate.

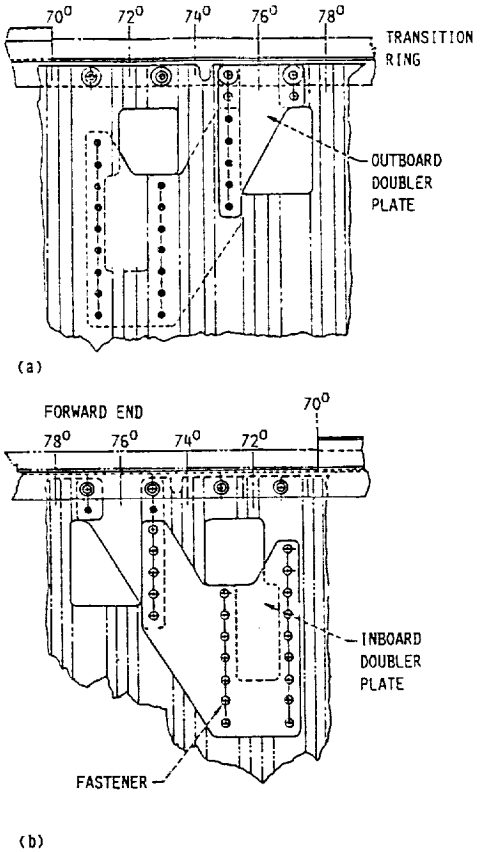

(a) View from outside cylinder.
(b) View from inside cylinder.

Figure 4.—Pneumatic line cutouts with doubler plates.

section. The G vehicle aft adapter was structurally identical to that of the G-Prime vehicle except that five separate graphite/epoxy panels were used instead of four. One of the original panels was split at a circumferential location to provide a gap for the LO_2 fill-and-drain line (fig. 10). This gap was similar to that provided for the LH_2 fill-and-drain line.

Composite Adapter Design Criteria

Design requirements.—The need for additional payload capability and a limitation on pyrotechnic separation ring temperature influenced the decision to use a graphite/epoxy composite material for the forward and aft adapters. The low-conductivity characteristic of graphite/epoxy composites reduced propellant boiloff, which translated into additional payload capability. The material's low density and high strength decreased structural weight, which also increased payload capability. Additionally, the low-conductivity characteristic was required for the aft adapter to maintain the pyrotechnic separation ring temperature within its operational limits.

General criteria.—The general design criteria were acquired from the space shuttle design criteria. The most directly applicable criteria were the following:

(1) Achieve an ultimate factor of safety of 1.4.
(2) Reduce Mil Handbook 5 bearing allowables by 15 percent.
(3) Use a 1.20 fitting factor for all fittings.
(4) Use the smaller of mean thickness or 1.05 times minimum tolerance thickness for analytical stability thickness.

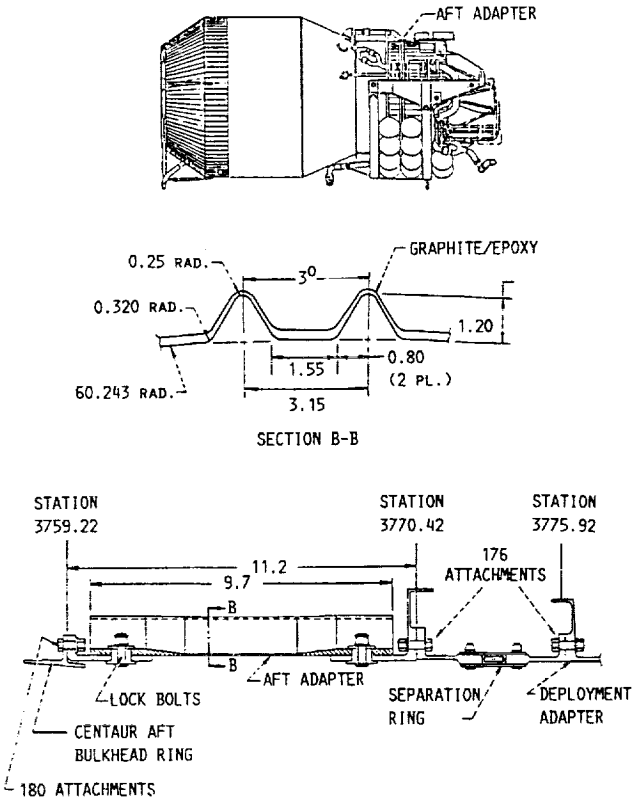

Figure 5. —G-Prime vehicle aft adapter (dimensions in inches).

(5) Use the smaller of mean thickness or 1.10 times minimum tolerance thickness for analytical strength thickness.
(6) Use A-basis material allowables for single load path structures.
(7) Use B-basis material allowables for redundant structures.

Other general design criteria that were applied specifically to the composite adapters included the rule that no buckling is permitted up to ultimate load. Buckling of the shuttle/Centaur composite adapters was not a major design driver so that the no-buckling rule had minimal effect on weight.

Nominal ply thickness values were used for analytical purposes. These were assumed to be 0.005 in. per ply for the tape and 0.013 in. per ply for the cloth. Because a tolerance callout is not normally applied to a ply, 0.0005 in. is sometimes subtracted from the nominal dimension for analysis purposes. This was not necessary for the shuttle/Centaur adapters because of the thickness criteria noted in items 4 and 5 listed at the beginning of this subsection.

The presence of 0.005-in. fiberglass surface plies applied in some areas for manufacturing and dissimilar material separation purposes was ignored in all strength and stiffness calculations. For example, integral fiberglass patches were located at each graphite/epoxy-panel-to-ring-fastener location to separate the graphite fibers from the mating aluminum ring and to improve the quality of drilled holes in the graphite/epoxy. These patches were ignored in the strength and stiffness analyses because of their discontinuous nature. Static electric conduction paths were provided by thin aluminum foil strips bonded to the flats of selected corrugations. These were also ignored in the analyses.

Material allowables.—The material used for the shuttle/Centaur adapters was T300/934 graphite/epoxy. Although this material is used extensively, no commonly accepted material properties were documented in standard publications such as Mil Handbooks 17 and 23. Hence, material properties were obtained from numerous coupon tests that employed the laminate layups selected for the individual adapters.

Lamina properties shown in table I were statistically derived by using standard methods or an altered method commonly referred to as the B.H. Jones technique (ref. 1). Strain allowables were A basis in nature and were set no higher than the lowest

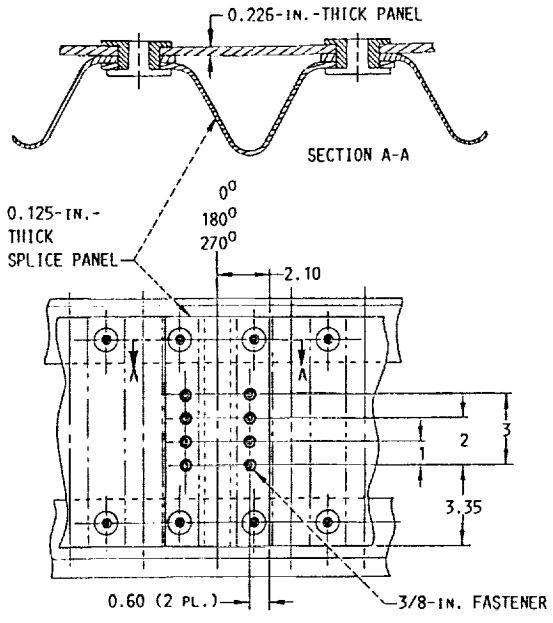

Figure 6.—Splice panel at 0°, 180°, and 270° (dimensions in inches).

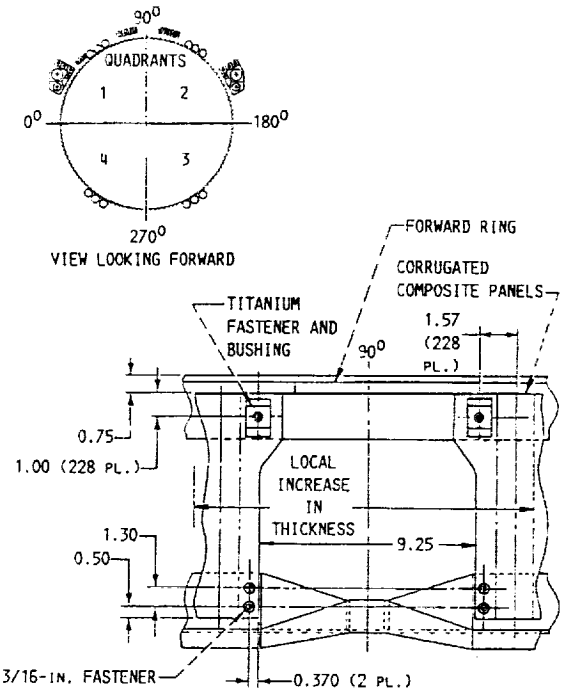

Figure 7.—LH_2 cutout at 90° (dimensions in inches).

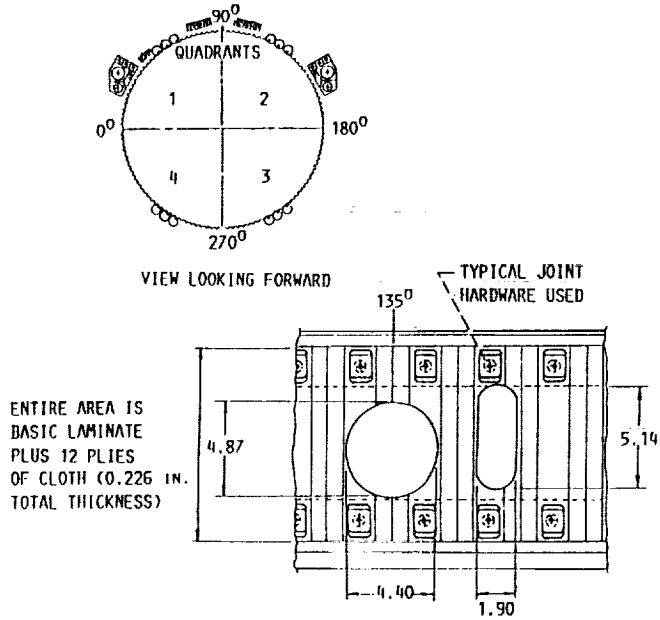

Figure 8.—LO_2 vent line and instrumentation cutouts at 135° (dimensions in inches).

test data point. Stiffness properties were average values. Some small adjustments were made in some instances to both strength and stiffness lamina values to allow better correlation with G-Prime and G vehicle laminate test data.

Table II summarizes the laminate properties obtained from a standard laminate properties computer program. The lamina data of table I were used as input to the program for the various ply layups. The laminate selection for the G-Prime vehicle forward

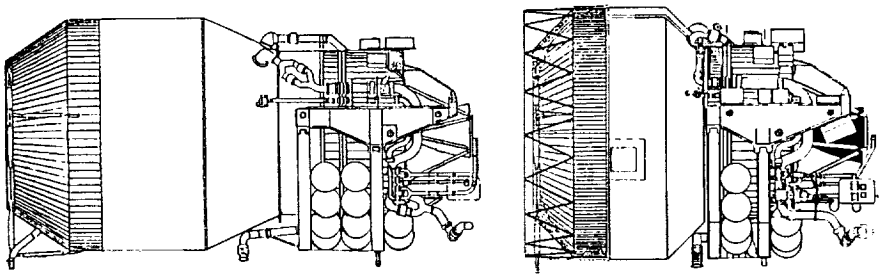

G-PRIME VEHICLE G VEHICLE

	G-PRIME VEHICLE	G VEHICLE
LENGTH, FT	30	20
FORWARD ADAPTER CONE, DEG	56.7	46.9
LH_2 TANK CONE, DEG	24	45
CENTAUR SUPPORT SYSTEM (CSS) PIN-TO-PIN, IN.	102.26	70.80
CSS He BOTTLES	20	12
FORWARD BULKHEAD MAJOR-TO-MINOR DIAMETER RATIO A/B	1.38	1.58
DRY WEIGHT (VEHICLE), LB	6088	6750
TANKED WEIGHT (VEHICLE), LB	50 270	37 319
CENTAUR INTEGRATED SUPPORT SYSTEM (CISS) WEIGHT, LB	6528	6497

Figure 9.—Comparison of Centaur G-Prime and G vehicles.

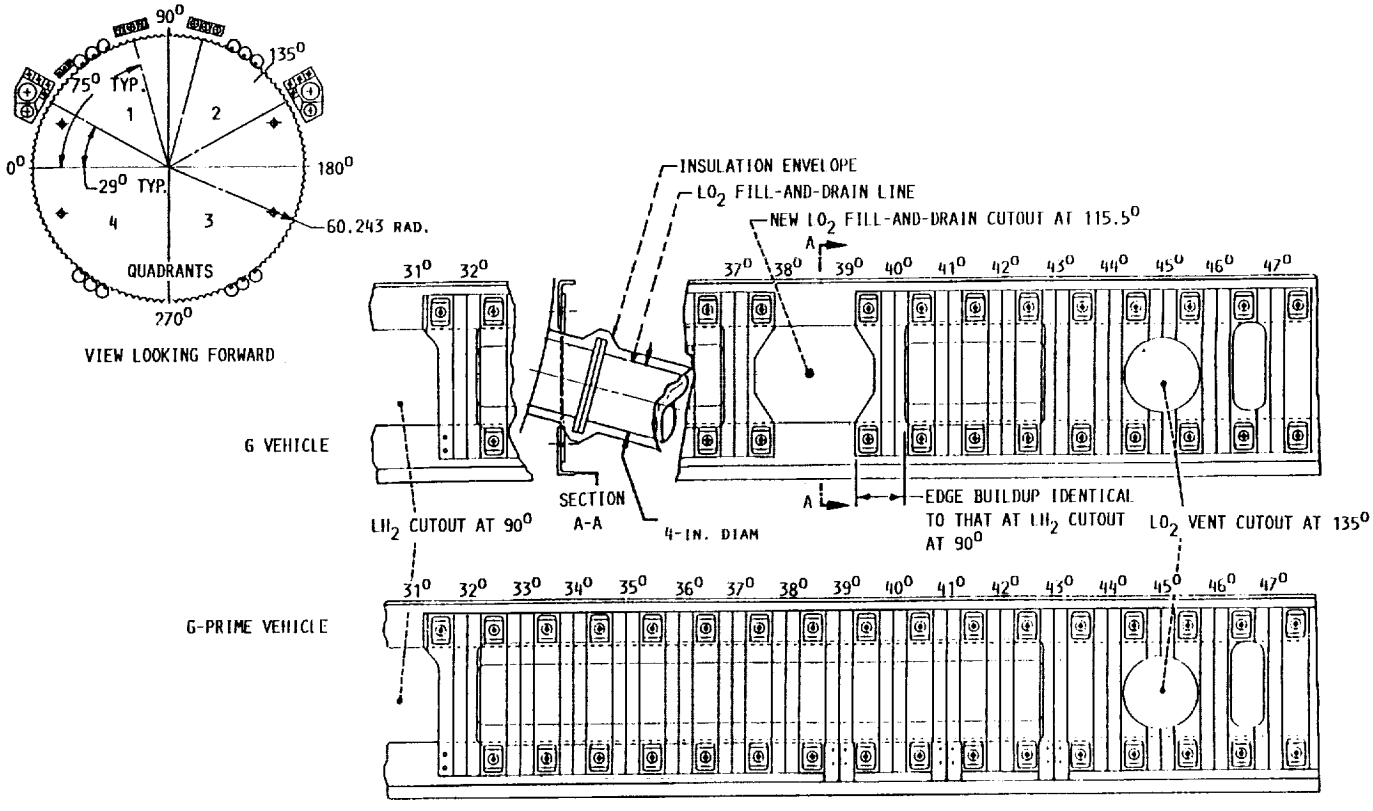

Figure 10.—LO_2 fill-and-drain cutout.

TABLE I.—SHUTTLE/CENTAUR COMPOSITE ADAPTER LAMINA PROPERTIES

Lamina property	Tape[a]		Cloth[b]	
	Room temperature	Cryogenic temperature	Room temperature	Cryogenic temperature
Longitudinal modulus of elasticity, E_{11}, msi				
Tension	19.4	19.7	10.1	---
Compression	17.8	18.7	----	---
Lateral modulus of elasticity, E_{22}, msi	1.5	2.5	9.6	---
Poisson's ratio, ν_{12}	0.3	0.3	0.05	---
Shear modulus, G_{12}	0.71	1.5	0.66	---
Longitudinal strain, e_{11}, in./in.				
Tension	0.0064	0.0047	(c)	(c)
Compression	−0.0081	−0.0091	↓	↓
Lateral strain, e_{22}, in./in.	±0.1	±0.1		
Shear strain, γ_{22}, in./in.	±0.0140	±0.0110		
Longitudinal coefficient of expansion, α_x, μin./in./°F	−0.3	------	1.2	---
Lateral coefficient of expansion, α_y, μin./in./°F	15.0	------	1.2	---

[a]Lamina thickness t, 0.0050 in.
[b]Lamina thickness t, 0.0130 in.
[c]Use tape values, maintain good safety margins.

TABLE II.—BASIC SHELL LAMINATE PROPERTIES

[0° direction (x) parallel to corrugations.]

Laminate property	Adapter					
	G forward[a]		G/G-Prime aft[b]		G-Prime forward[c]	
	Room temperature	Cryogenic temperature	Room temperature	Cryogenic temperature	Room temperature	Cryogenic temperature
Longitudinal modulus of elasticity, E_x, msi						
Tension	11.5	12.3	7.00	8.04	6.52	7.57
Compression	10.6	11.8	6.51	7.73	6.88	7.29
Lateral modulus of elasticity, E_y, msi						
Tension	5.78	6.77	8.80	9.80	9.37	10.4
Compression	5.40	6.53	8.15	9.39	8.67	9.91
Poisson's ratio, ν_{xy}						
Tension	0.31	0.28	0.25	0.23	0.23	0.22
Compression	0.31	0.28	0.25	0.23	0.23	0.22
Shear modulus, G_{xy}						
Tension	2.15	2.74	2.66	3.18	2.62	3.15
Compression	2.02	2.66	2.48	3.07	2.44	3.04
Longitudinal coefficient of expansion, α_x, μin./in./°F						
Tension	0.29	0.69	1.46	2.33	1.73	2.67
Compression	0.34	0.75	1.60	2.43	1.88	2.79
Lateral coefficient of expansion, α_y, μin./in./°F						
Tension	2.43	3.61	0.74	1.35	0.57	1.12
Compression	2.62	3.75	0.82	1.43	0.65	1.19
Ultimate σ_x, ksi						
Tension	73.6	57.9	44.8	37.8	41.7	35.6
Compression	85.9	101	52.7	70.4	38.9	34.3
Ultimate σ_y, ksi						
Tension	37.0	31.8	61.4	50.2	59.9	48.6
Compression	43.7	59.5	72.0	84.8	55.5	46.6
Ultimate shear strength, ksi						
Tension	±27.5	±25.8	±35.0	±31.0	±35.7	±31.5
Compression	±25.8	±25.0	±32.7	±29.9	±33.3	±30.4

[a]$[0/\pm 45/0/90/0]_s$; thickness t, 0.060 in.
[b]$[\pm 55/0_2/\pm 75]/\pm 55/[s]$; thickness t, 0.070 in.
[c]$[55/125/0/90]_s$; thickness t, 0.040 in.

adapter was made on the basis of stability requirements alone by using the computer code STAGSC (Structural Analysis of General Shells in Compression). Therefore, only material stiffness properties were needed. Testing proved the panel to be quite stable at ultimate load so that the true design driver was minimum practical gage (0.040 in.).

Failure criteria.—For basic laminate point stress analysis, the first ply maximum strain criterion was used; that is, macromechanics analysis techniques established the maximum laminate strains (e_{11}, e_{22}, γ_{12}) in each ply for a given load condition. Failure of the entire laminate occurred when any ply reached one of the allowable strain values shown in table I. This method depends on basic allowables established through lamina tests. For the shuttle/Centaur project, however, both lamina and laminate testing were used to establish strain allowables, thereby increasing confidence in the values used for the failure criteria.

The in-plane matrix direction strain allowable shown in table I was established at an arbitrarily high value of 0.10 in./in. Matrix failure was not considered in the laminate analyses of the shuttle/Centaur adapters. Matrix strain allowables normally acquired from transverse tests of undirectional samples usually result in low strains and much data scatter. Using these data for strain allowables results in laminates that are theoretically weak in the matrix direction of a ply. Test results, however, do not sustain these predictions because the weak matrix direction of a ply is strengthened by the presence of an overlapping angle ply.

In addition to in-plane matrix failure, interlaminar shear and normal tension were given consideration; but it was determined that no satisfactory method was available to obtain reliable allowable strength values. Attempts were made to devise a method for establishing allowable strength values for these failure modes that were applicable to the shuttle/Centaur corrugations. The data obtained were erratic. Therefore, without a reliable allowable strength value, no justification existed to perform detailed analyses of these matrix failure modes. Consequently, superficial analyses were performed by using lower bound data as allowables. Primary strength confirmation was achieved by subcomponent testing.

Failure due to fatigue loading was considered even though the shuttle/Centaur is normally subjected to one launch environment only, or possibly two in the event of an aborted mission with subsequent relaunch. A typical launch vibratory loading spectrum was established for the shuttle/Centaur vehicle on the basis of dynamic analyses. Data from the literature showed that the expected fatigue loading would not cause a failure in the composite. However, some questions remained with regard to cyclic damage at cryogenic temperature. The microevents which reduce the strength and stiffness and which determine the life of a composite laminate are complex, various, and intricately related to a variety of failure modes under different circumstances. Consequently, analytical techniques for predicting life are difficult to derive. To address the concern of fatigue damage, fatigue cycling was included as part of the design verification tests.

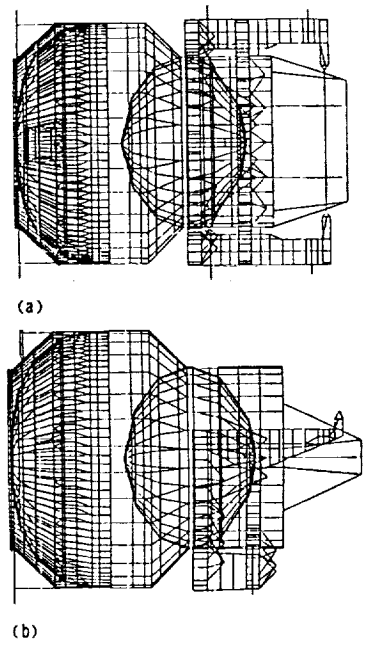

(a) View looking down.
(b) View looking inboard (left side).

Figure 11.—G vehicle integrated finite element model (2800 grids, 5900 elements).

Load Analyses

Overall integrated model.—The stress analysis of the composite adapters began at the global level with overall integrated finite element models (figs. 11 and 12). The entire vehicle was modeled with appropriate plate and shell elements. The corrugated adapters were represented by shell elements with smeared orthotropic material properties obtained from a lamina properties computer program and specimen tests that provided circumferential stiffness of the corrugations. The integrated model provided internal loads for a multitude of

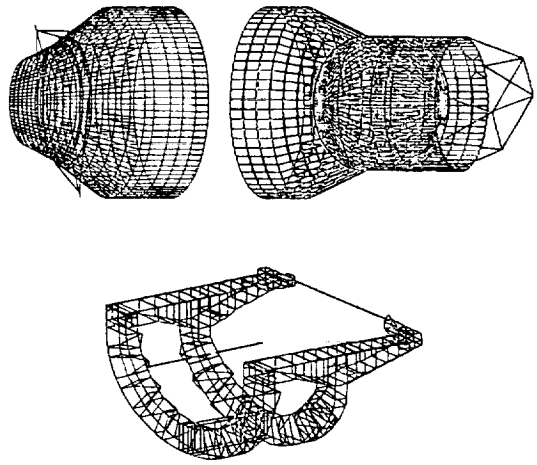

Figure 12.—G-Prime vehicle integrated finite element model.

load cases. Axial and shear loads were extracted from these models for further detailed stress analysis.

G-Prime loads.—No attempt was made to analyze the composite adapters for all the individual load cases. Plots of load as a function of circumferential location were made for all load cases run with the global model. The upper and lower bound loads at each angular position along the circumference were identified. These points were then connected to form an upper and lower bound curve that enveloped all load cases. Typical shear and axial load envelope curves are shown in figure 13. The corresponding axial and shear loads at each angular position were plotted to form an interaction load plot. These points were then enveloped to form limit and ultimate design load curves as shown in figures 14 and 15.

G loads.—Loads for the G vehicle aft adapter were generated in a similar manner as those generated for the G-Prime vehicle aft adapter. As shown in figure 13, the G and G-Prime vehicle load envelopes were similar, but the G vehicle loads were significantly lower at the peaks. On the basis of this information, it was concluded that the G-Prime vehicle composite aft adapter design was acceptable for application to the G vehicle. Because of the lower peak loads, it would have been possible to remove some weight from the aft adapter, but it was decided that the weight savings was not significant enough for a design change. Commonality of design presented numerous advantages.

Loads for the G vehicle forward adapter design were dictated by the 22 hardpoints needed for attachment of the payload truss shown in figure 9. Various load cases were run by using the G vehicle integrated model, which provided loads at the hardpoints. The loads were plotted on a load-shear interaction diagram and enveloped as shown in figure 16. Since the hardpoint loads resulted from body axial and bending loads, some hardpoints were loaded more than others. However, each hardpoint was designed to be capable of sustaining the maximum load contained within the load envelope. This did not mean that the payload capability of the G vehicle was 22 times the load capability of a typical hardpoint. Each payload had to be considered on an individual basis to establish that payload's load application characteristics on the entire vehicle.

Subcomponent Design Evaluation Tests

A major part of the development of the shuttle/Centaur composite adapters was the performance of a multitude of design evaluation tests to augment analyses. Tests were performed in-house at General Dynamics Space Systems Division (GDSSD); and at McDonnell Douglas Aircraft in St. Louis, Missouri, and Northrup Corporation in Hawthorne, California, under subcontract to GDSSD. Unique equipment that allowed combined loading of test panels required the services of the two subcontractors noted. The following gives a description of these tests and a summary of results.

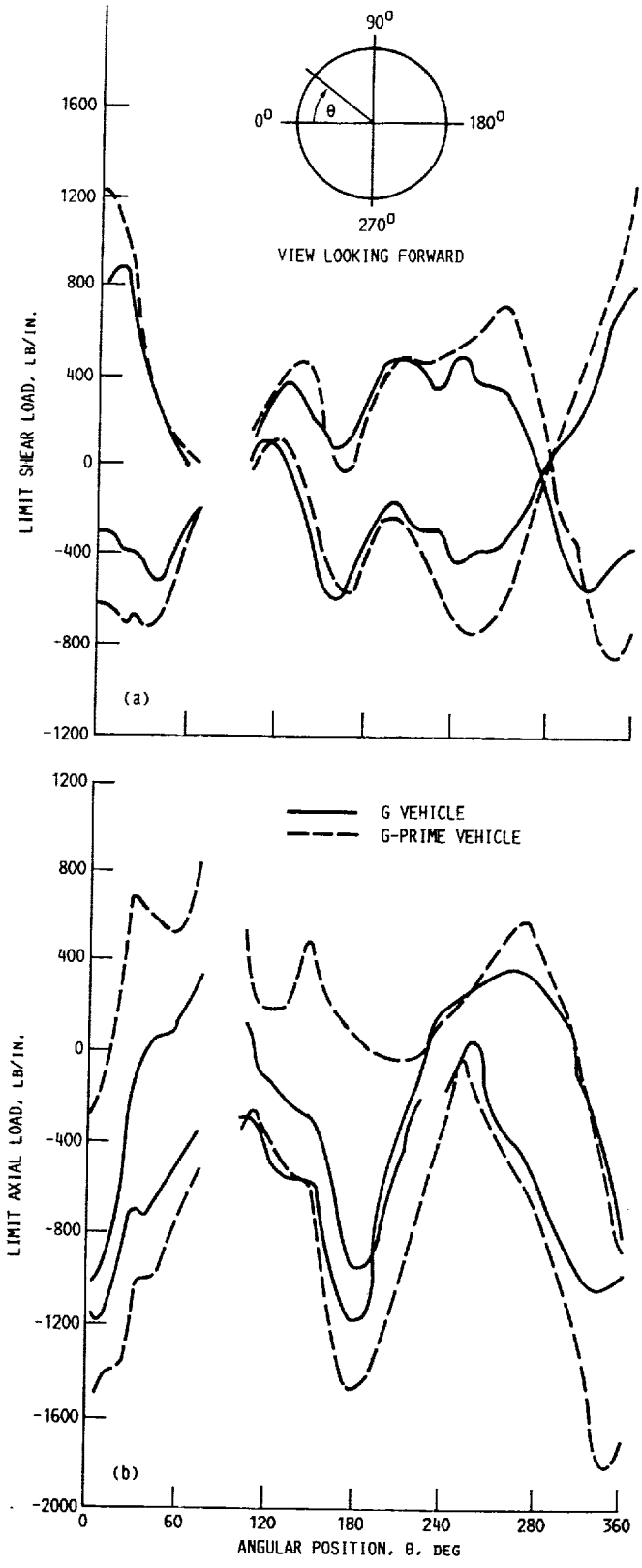

(a) Limit shear load.
(b) Limit axial load.

Figure 13.—G-Prime and G vehicle aft adapter load envelopes.

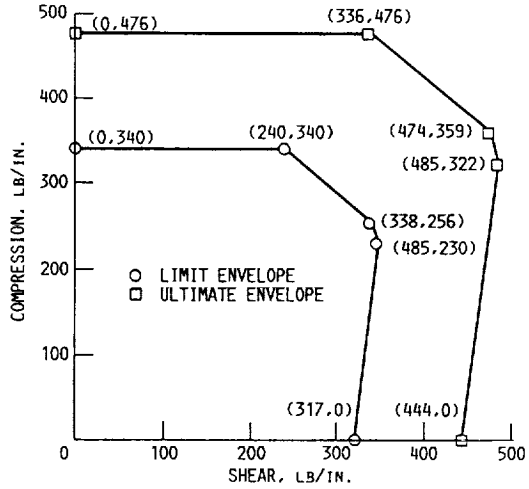

Figure 14.—G-Prime vehicle forward adapter design loads (panel FA3).

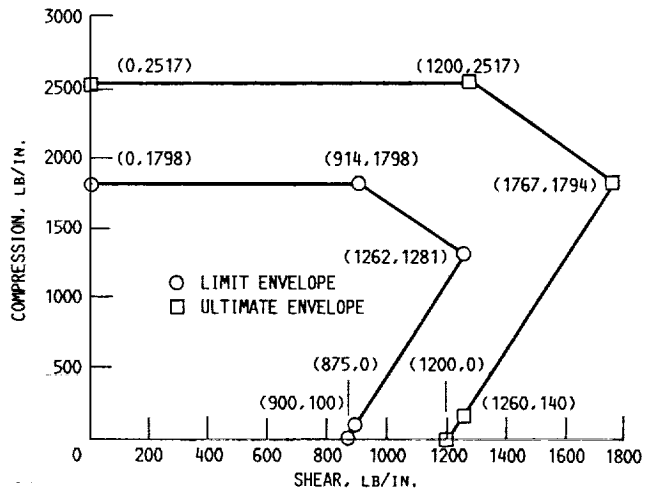

Figure 15.—G-Prime vehicle aft adapter design loads.

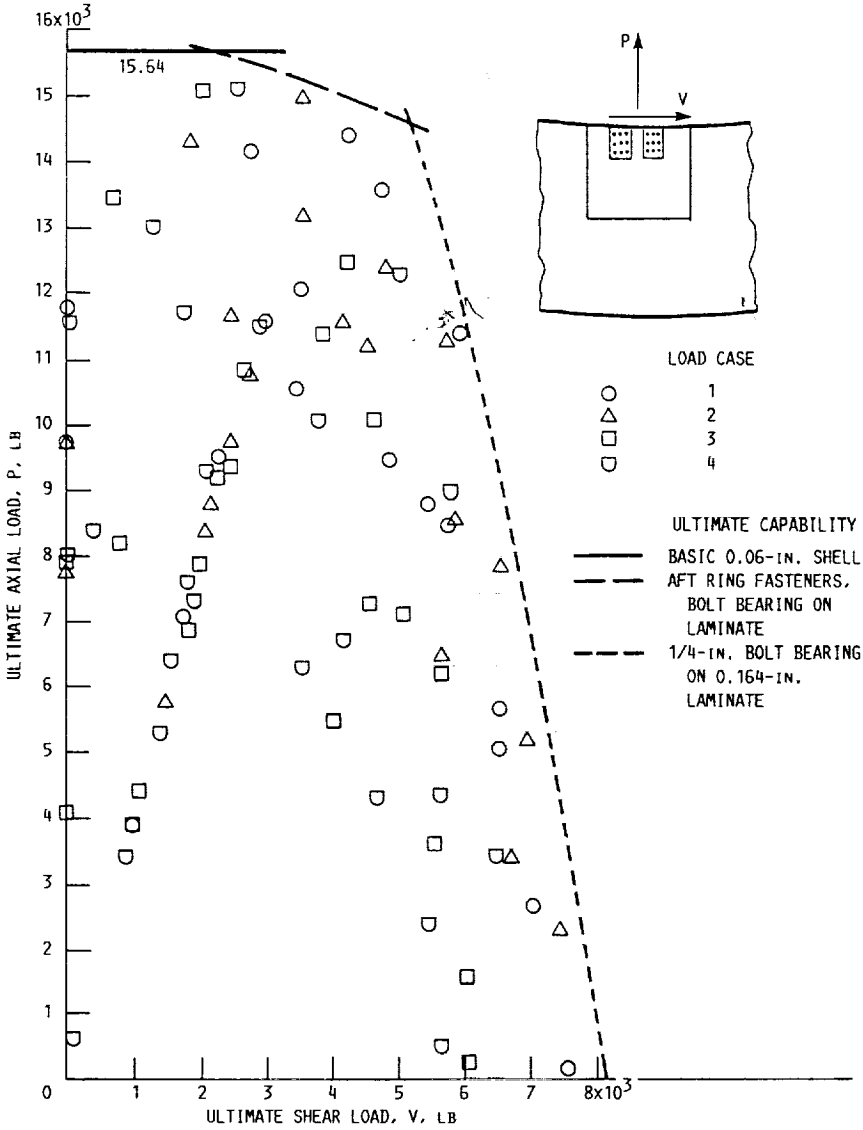

Figure 16.—G vehicle hardpoint ultimate load curve.

GDSSD G-Prime Subcomponent Tests

These tests involved representative portions of both the forward and aft composite adapters. Figure 17 shows six types of specimens and the area of the adapter they represented. Table III summarizes the results. A brief description of each test follows.

End flex specimen.—The purpose of this test was to determine the circumferential stiffness of the corrugations and their ability to flex without incurring any damage. It was calculated that the required circumferential deflection for each corrugation to accommodate tank cooldown was 0.012 in. The end flexure specimen was cooled to −320 °F, and the load was measured for deflections of 0.012 and 0.036 in. Table III shows that the corrugation stiffnesses measured for the aft and forward adapters were 330 and 1470 lb/in., respectively.

Compression panel.—The compression panel specimens consisted of test panels that were the actual length of the forward and aft adapters. Each panel had four corrugations, and the end buildup, end rings, and fasteners were duplicated. Each panel was loaded in compression to failure at room temperature. The failure loads for the forward and aft adapters were 7000 and 20 750 lb, respectively. The design loads for each panel were 5250 lb for the forward panel and 20 000 lb for the aft panel. Failure occurred as a bearing failure in the buildup fastener area.

Crippling test.—The purpose of the crippling test was to measure the crippling strength of the basic skin thickness corrugations. Test specimens four corrugations wide and 7.5 in. long were compression tested. The forward adapter specimens had a basic skin thickness of 0.040 in., and the aft adapter specimens had a basic skin thickness of 0.070 in. The specimens had no buildup on the ends and were potted into a metal channel at each end. The crippling strengths of both adapter specimens were well above the design crippling strengths.

End joint compression test.—The end joint compression test was performed to develop the required end buildup and the fastener size. Several iterations were required for the aft adapter before an acceptable configuration was attained. The specimens consisted of 2½ corrugations fastened to a simulated ring at one end with two fasteners. The opposite end was potted into a metal channel. The specimens were short enough to preclude a buckling failure and to ensure a fastener hole bearing failure in the composite. As shown in table III, several tests were run with aft adapter specimens at room temperature and at −320 °F.

End joint tension test.—The specimens used for this test consisted of an aluminum strip representing the ring and a composite strip representing the buildup flat region of a corrugation. The specimens were joined with a typical fastener and loaded in tension to failure. Tests were run at room temperature and at −320 °F. In all cases the failure load was considerably greater than the design load. The failure usually occurred as a bearing failure in the fastener region.

Shear panel tests.—The shear panel tests were performed to evaluate the shear strength and shear stability of the corrugations. The test specimen was adapted to what is commonly referred

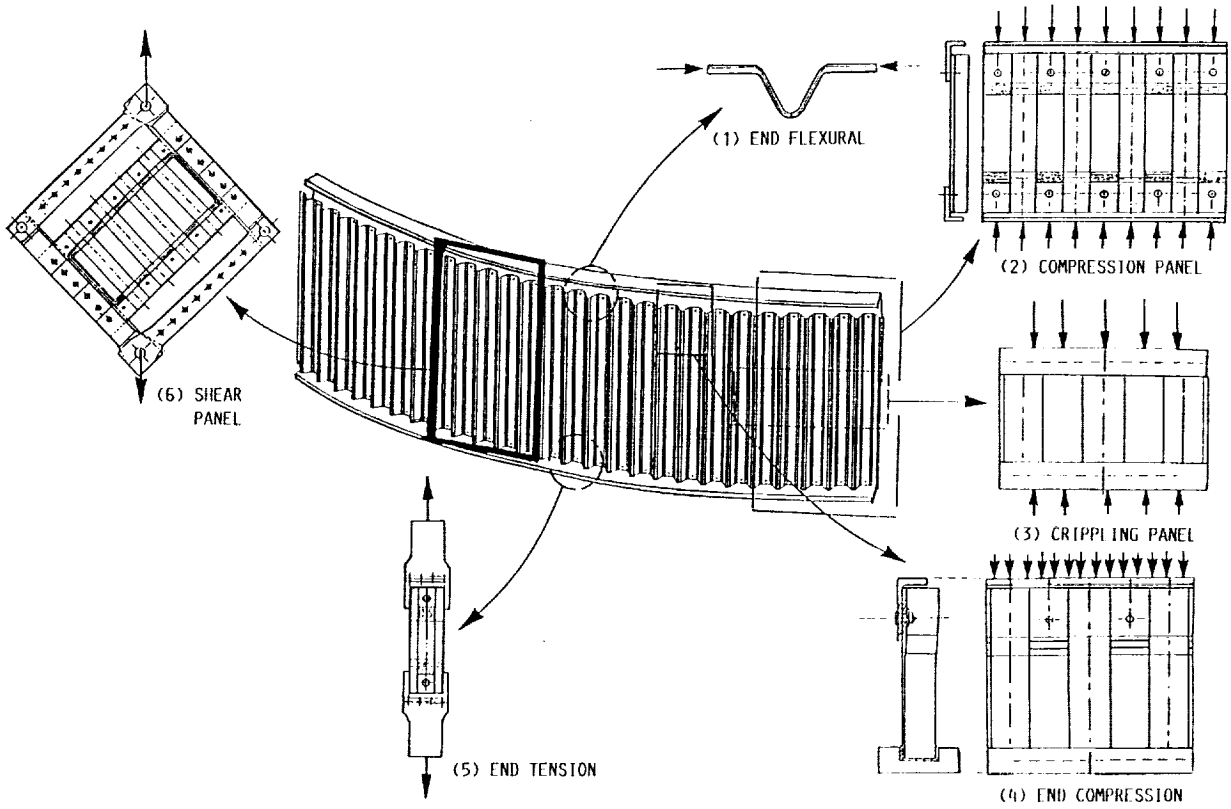

Figure 17.—Subcomponent testing configurations.

TABLE III.—SUBCOMPONENT TEST SUMMARY

Specimen number	Test type	Design load, lb	Failure load, lb	Test temperature, °F	Comments
1	Aft end flex	------	No failure	−320	Spring rate, 1470 lb/in.
2	Forward end flex	------	No failure	−320	Spring rate, 330 lb/in.
3	Compression	30 000	24 380	Room	Insufficient edge support, local failure
	Compression	20 000	20 750		Retest after trimming off damaged edge
4	Cripple	30 000	50 000		Specimen strength exceeded test machine
	Cripple	30 000	60 700		Larger test machine
5	Cripple	30 000	61 400		
6	Compression	7 000	7 580		Insufficient edge support, local failure
	Compression	5 250	7 000		Retest split-tube edge support
7	Cripple	7 000	26 000		
8	Cripple	7 000	28 600		Initial buckling, 22 000 lb
9	Shear	32 000	33 700		New design of layup at end buildup
10	Shear	8 400	9 960		Bad test—wrong washers under fastener
11	Shear	8 400	12 750		
12	End compression	14 000	14 375		
13	↓	19 200	19 650		
14	↓	↓	16 500		
15	↓	↓	26 000	↓	Steel end angle
16	↓	↓	22 800	−320	Aluminum end angle
17	↓	↓	15 500	Room	Aluminum end angle
18	↓	3 400	6 280	↓	
19	↓	3 400	5 900	↓	
20	End tension	1 900	6 675	↓	
21	↓	↓	5 500	−320	Grip failure, no failure near test end
22	↓	↓	4 880	−320	Grip failure, no failure near test end
23	↓	↓	4 600	−320	Grip failure, no failure near test end
24	↓	1 300	2 755	Room	
25	↓	↓	2 800	−320	
26	↓	↓	2 580	−320	
27	↓	↓	2 660	−320	

to as a "picture frame" test fixture. The specimen was attached within the frame, which had hinged corners. Applying a tensile force to two opposite corners of the frame produced a shear load on the test specimen. Test specimen panels representing the forward and aft adapters were tested. Results showed that the corrugated panels had adequate shear strength but that the shear distribution was not uniform because of the nature of the test setup. The corners of the test panels were subjected to a shear stress that was approximately three times that at the center. As a result, an alternative test method was investigated. This resulted in using a combined compression-shear test facility located at McDonnell Douglas Aircraft (McAir).

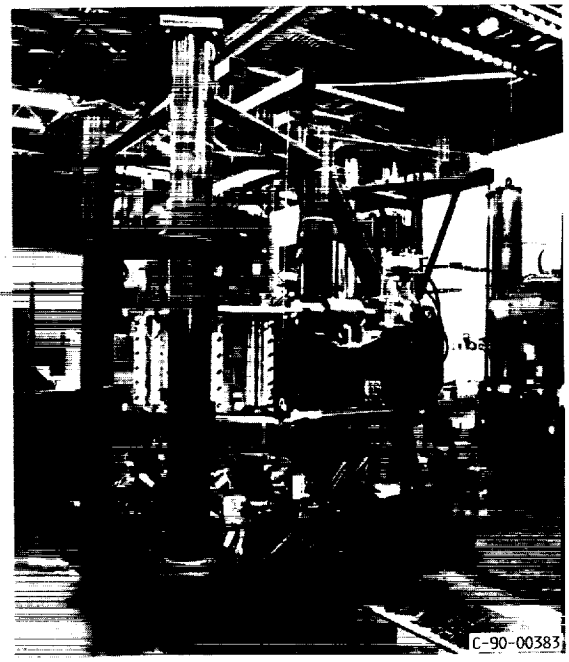

Figure 18.—McAir compression/shear test machine.

McDonnell Douglas Aircraft (McAir) G-Prime Combined Compression/Shear Load Tests

The McDonnell Douglas combined compression/shear load test machine is shown in figure 18. Figures 19 and 20 show the manner in which the combined load was applied to the adapter specimens. The compression load was applied by hydraulic cylinders located below the test section and transmitted by three

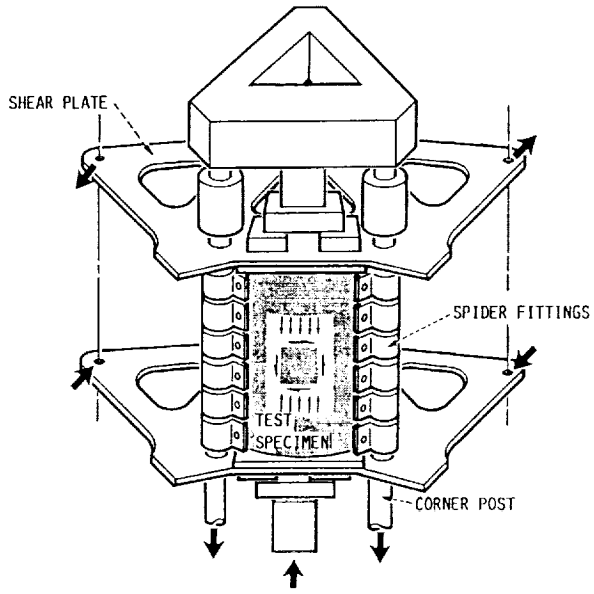

Figure 19.—Schematic of McAir load application method.

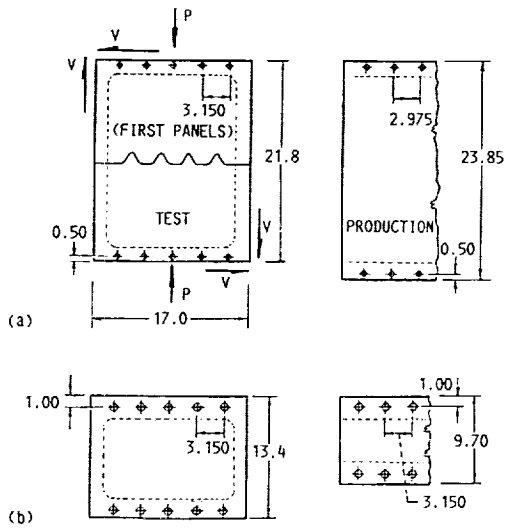

(a) Forward adapter.
(b) Aft adapter.

Figure 21.—McAir G-Prime vehicle test panels (dimensions in inches).

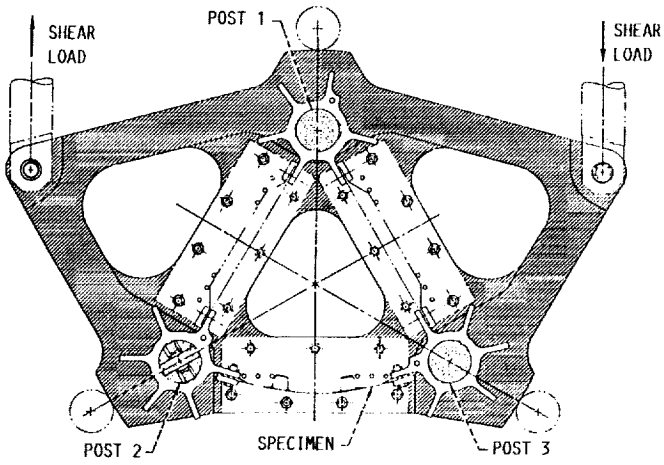

Figure 20.—Shear plate and specimen end attachment.

corner posts to the top of the test section. Slip fit "spider fittings" on each post provided attachment points for the test panel and two dummy panels, forming a triangular torque box. The panels were also attached to the stationary lower reaction plate and the movable upper plate. Torque was applied to the triangular torque box by two hydraulic cylinders connected to the upper plate, thereby transmitting a shear load into the panels. Universal joints in each corner post permitted the shear load to be applied in addition to the compressive load.

Two forward adapter panels and two aft adapter panels were tested. Because of machine limitations, the test panel lengths could not be identical to the production panel lengths, as shown in figure 21. Each panel was tested by a systematic loading sequence that subjected it to key points on its limit and ultimate design envelopes (figs. 14 and 15). Each point on the load envelopes was approached by applying first the compressive load and then the shear load. This was required to control the lifting tendency of the torque box when shear was applied.

Table IV shows the results of the McAir panel tests. All load points were achieved on the design envelopes shown in figures 14 and 15 before loading the panels to failure. The test

TABLE IV.—McAIR COMBINED COMPRESSION/SHEAR FAILURE LOADS

Panel		Compression				Shear			
Type	Number	Applied force, lb	Estimated force per corrugation, lb	N_x, lb/in.		Failure force, lb	Force per corrugation, lb	N_{xy}, lb/in.	
				Test value	Ultimate design			Test value	Ultimate design
Forward	FA1	5 900	944	300	476	8 574	1777	564	484
	FA2	7 400	1184	376	476	8 614	1786	567	484
Aft	AA5	46 325	7238	2289	2517	37 271	7724	2452	1767
	AA6	41 918	6550	2079	2517	34 030	7053	2239	1767

compression/shear failure loads fell outside their respective ultimate design envelopes. These loads are plotted in figures 22 and 23 to show their relationship to the design envelopes.

Failure of the test panels usually occurred in the fastener region. The corrugated construction was inherently weak in transmitting a smooth shear flow from a corrugation into its single fastener. Shear flow through the corrugation ends caused a local bending moment that resulted in a tear-out force in the fastener region. The original design used round washers under the fastener heads and caused a cutting action which resulted in premature failures in earlier adapter test panels. Square washers which reduced the effect of the tear-out action were used on test panels AA5 and AA6 and were finally incorporated into the aft adapter design. Although forward adapter panels FA1 and FA2 were tested successfully with round washers, square washers were incorporated into the forward adapter design to provide an additional margin of safety.

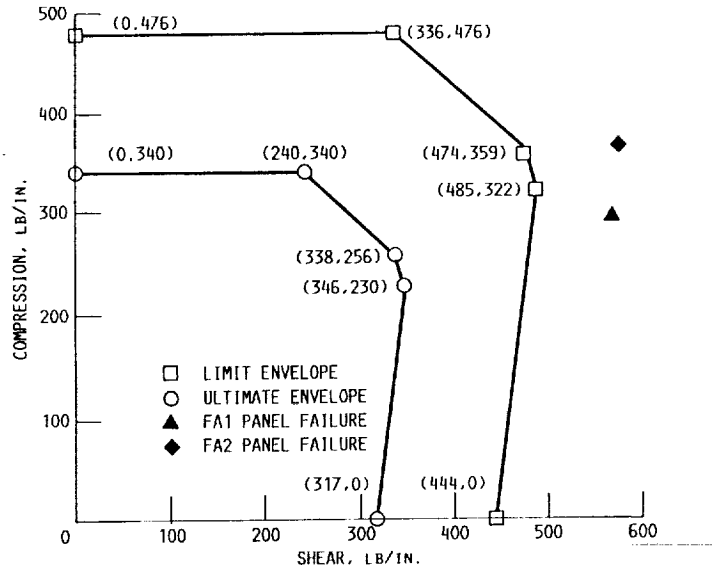

Figure 22.—Failure loads for forward adapter panels FA1 and FA2 compared with design load envelopes.

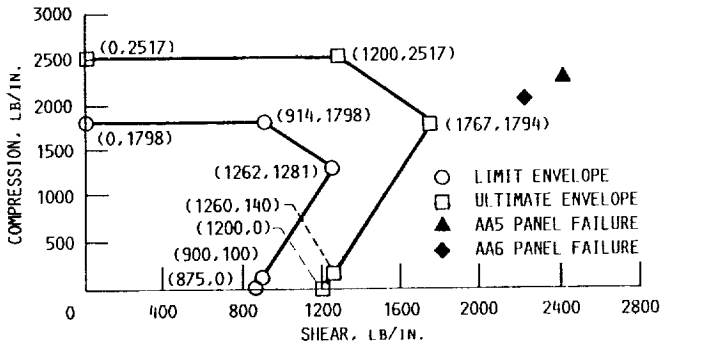

Figure 23.—Failure loads for aft adapter panels AA5 and AA6 compared with design load envelopes.

Northrup G-Prime Cutout Combined-Load Test

The machine used to load test the cutout areas of the forward and aft adapters (figs. 4 and 8) is shown in figure 24. It was not possible to run the cutout tests at McAir because the required test panel size was too large for their machine. The test panel size could not be reduced without causing the boundary constraints to overlap the zone being tested.

The Northrup machine in outward appearance was more simple in design than the McAir machine. The Northrup test machine had the advantage of combined tensile/shear and compression/shear load application capability, whereas the McAir test machine had only compression/shear capability. As in the McAir machine, the test specimen (forward or aft adapter panel) was part of a triangular torque box with two fiberglass honeycomb dummy panels, as shown in figure 24. Axial compression or tension load was applied at one end of the torque box by hydraulic cylinders and reacted at the opposite end by the fixed end plate. A disadvantage of the Northrup machine was that axial load would tend to collect in the stiff sections that joined the three panels together, and hence test loads had to be adjusted accordingly. (The McAir machine used noncontinuous corner members.) Two load cylinders produced a couple on the movable end plate which was transferred by pure torque through the test section into the fixed reaction end plate. The torque load set up the desired shear flow in the tripanel torque box. Lateral forces were prevented by a slotted hole in the loading frame support plate in which the loading frame shaft rested. The dead weight of the torque plate and other structures was offset by an auxiliary hydraulic cylinder. The desired input loading forces were manually controlled by controlling the hydraulic pressure. No load cells were used for early tests so that input loads were based on pressure and piston area.

The load envelopes used for the aft and forward adapter cutout areas and the test specimens are shown in figures 25 and 26, respectively. The anticipated flight loads for both adapters in the cutout areas were less than the maximum expected loads that occur away from the cutouts. Both tension/shear and compression/shear combined loads were applied. Just prior to reaching the final load point (1388-lb/in. shear, 1022-lb/in. axial loads) on the aft adapter ultimate load curve (fig. 25(b)), small cracks appeared at the edges of both cutouts, but the panel continued to carry load. The panel was then loaded to points (1100, −1628) and (946, −177) without further visible crack growth. The panel finally failed at point (1556,1175) by multiple large cracks at the cutout edges. Even though cracks were present at the cutout edges, the panel was capable of carrying ultimate design loads without complete failure.

The first forward adapter panel that was tested experienced a premature failure due to a tear-out around a fastener washer. The failure occurred at a fastener away from the cutout region and at a load combination inside the ultimate load envelope, as shown in figure 26(b). The test panel's round washers were made improperly with razor sharp edges, and they were

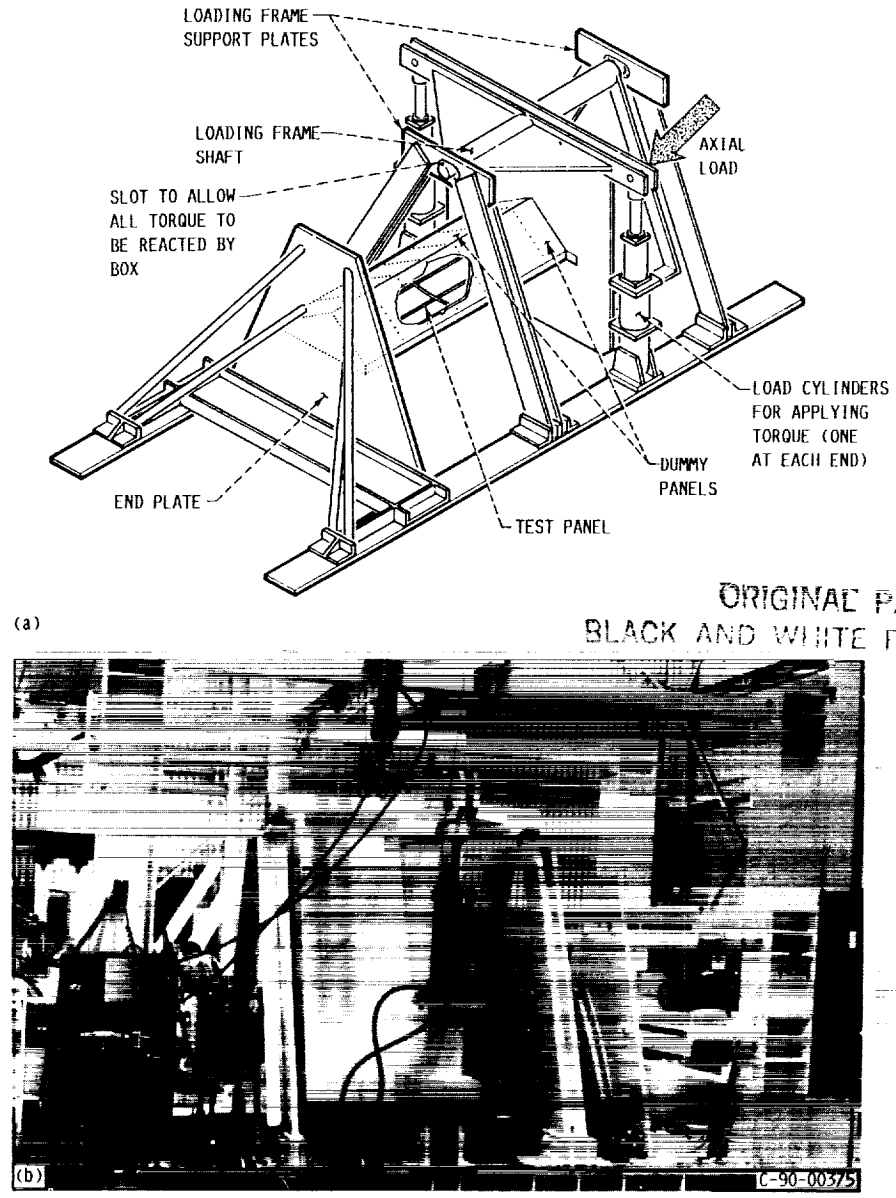

(a) Schematic.
(b) Side view.

Figure 24.—Northrup combined load test machine.

installed off-center. (This failure prompted a design change from round washers to square washers similar to those used for the aft adapter fasteners.) Another test panel was fabricated, and, in addition to the large cutouts, numerous small mounting bracket holes were included (0.204 in. diam. max.) to more closely simulate conditions surrounding the cutouts. Each labeled point on the limit and ultimate design envelope was repeated. The plan was then to apply a combined compressive and shear load that was 25 percent greater than the maximum ultimate compressive and shear loads. If the panel survived, a combined tension and shear load 25 percent greater than the maximum ultimate tension and shear loads was to be applied. The panel failed at 125 percent of the maximum ultimate compression load combined with 109 percent of the maximum ultimate shear load. Failure was a result of significant cutout free-edge buckling, which caused the laminate to crack. The addition of the small bracket holes appeared to have little effect on panel strength.

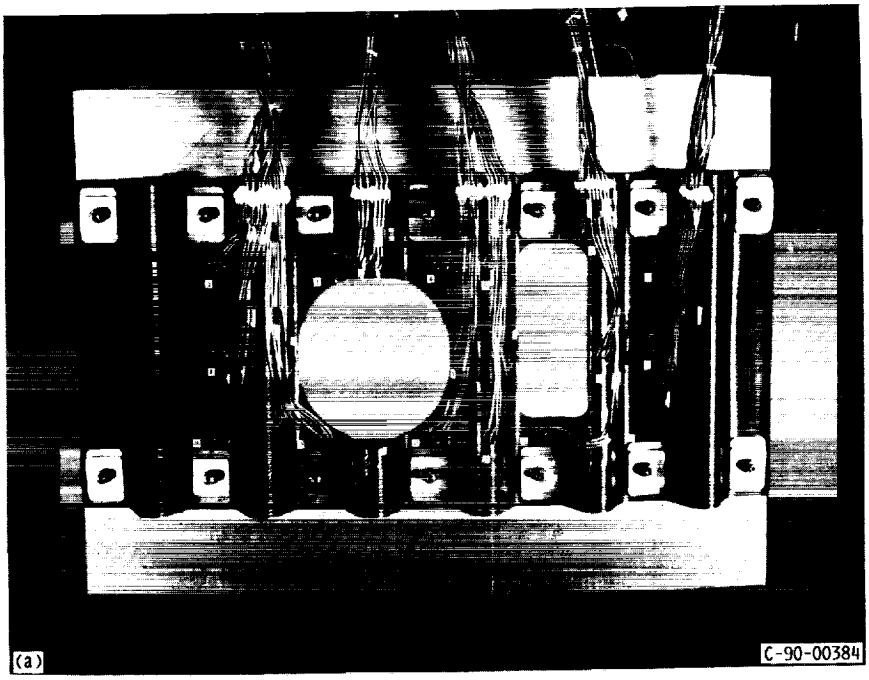

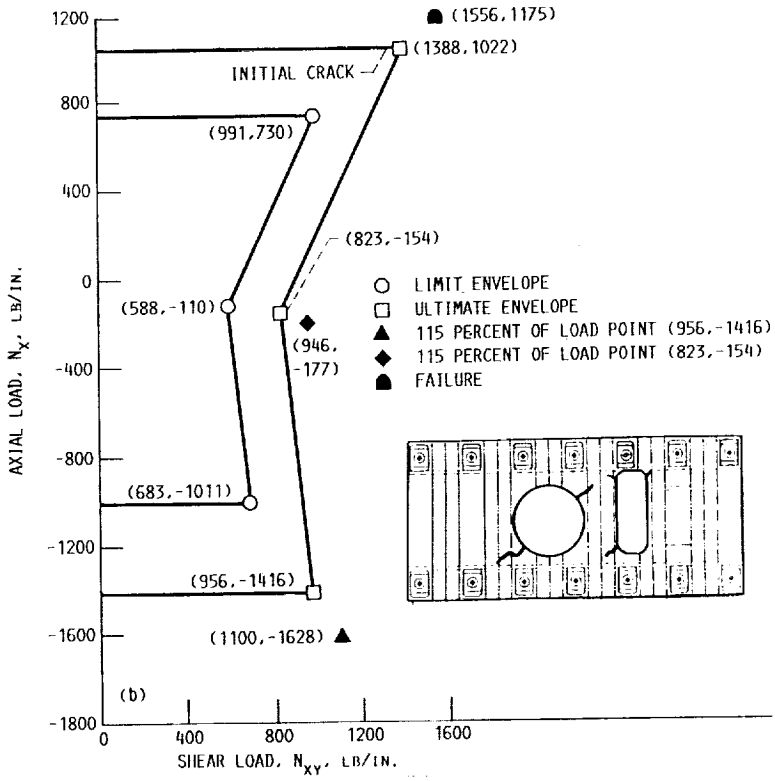

(a) Specimen.
(b) Load diagram.

Figure 25.—Aft adapter cutout test specimen and load diagram.

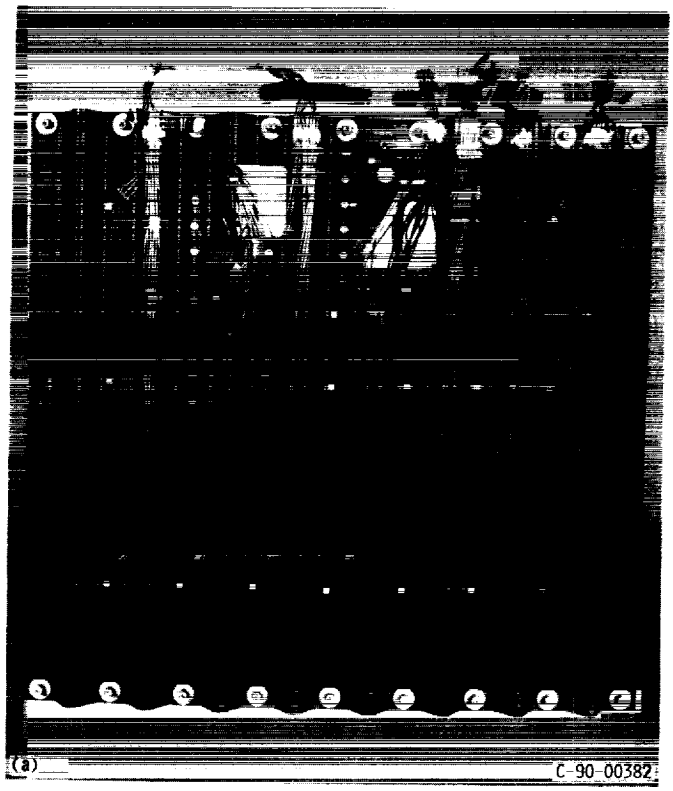

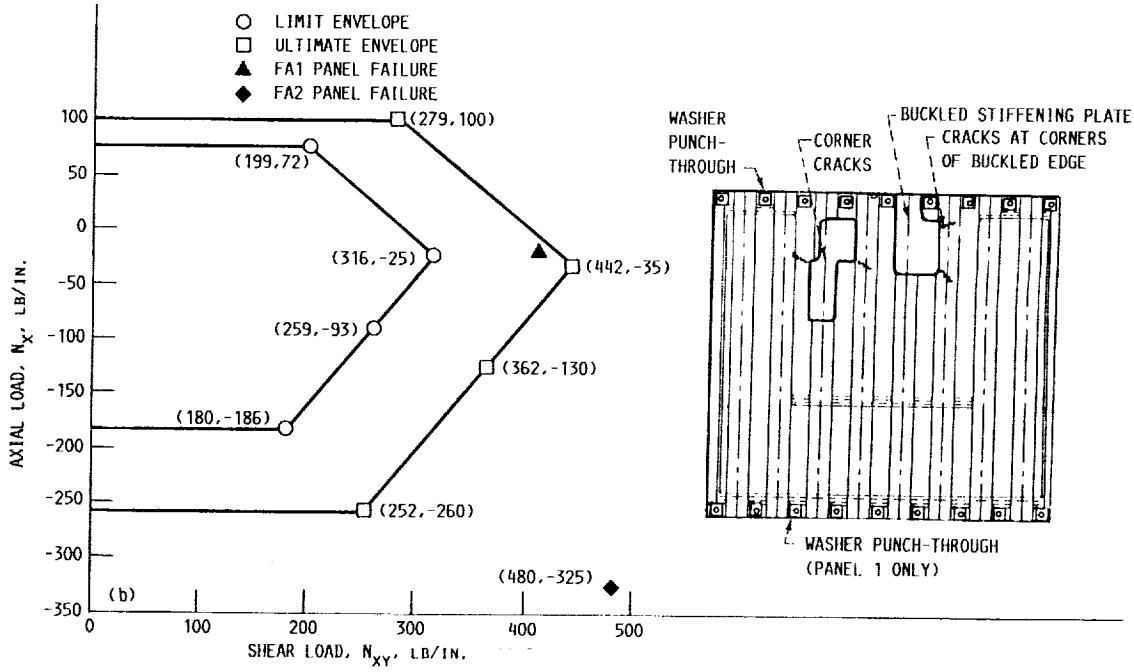

(a) Specimen.
(b) Load diagram.

Figure 26.—Forward adapter cutout test specimen and load diagram.

BLACK AND WHITE PHOTOGRAPH

Damage Tolerance Tests

Although all reasonable efforts were initiated to protect the composite adapters during fabrication and assembly, the possibility of damage was always prevalent. Visible damage can normally be repaired, but invisible damage and the integrity of repair methods were concerns. The production composite adapter panels were ultrasonically inspected following layup and cure, but no inspection other than visual was provided after the panels were assembled to the end rings and finally to the vehicle. It was impossible to constantly provide protection when match drilling holes between the panels and rings and when auxiliary equipment was assembled on the vehicle near the adapters. Proof testing was impractical because of the size of the adapters and the large combined compression/shear load needed to adequately duplicate service conditions. Consequently, a damage/repair test program was initiated to study the effect of invisible damage and repair techniques on composite panel strength. The concern was whether or not threshold (maximum size) invisible damage would grow to a critical stage when subjected to the launch vibration environment.

The damage tolerance/repair test plan consisted of two phases. Phase I was the compression testing of damaged, undamaged, and damaged and repaired corrugated test specimens at room temperature and at −423 °F. Nine two-corrugation, 17-in.-long specimens similar to the one shown in figure 27 were tested. Five specimens were tested at room temperature and four at −423 °F. Two of the room-temperature specimens had no damage, two had invisible impact damage, and one had damage that was repaired with a patch. The specimens tested at cryogenic temperature consisted of one with no damage, two with invisible impact damage, and one with a repaired damaged area. The damaged and undamaged room-temperature specimens were tested first to failure. This was done to establish a baseline. The cryogenic test specimens were tested to failure inside a cryostat, and the results were compared with the ambient results to determine if any correction factor should be applied to the phase II McAir damage tolerance tests, which are discussed later in this section.

Table V summarizes the results of the phase I tests. In the table, buckling load refers to the load at which incipient buckling occurred. The failure load was the load at which the panel could no longer carry any load. The three undamaged panels (1, 2, and 3) showed that the panel tested at cryogenic temperature was stronger than the two tested at room temperature. This was expected because theoretical and small specimen results showed Young's modulus to be higher at cryogenic temperature. The four damaged panels, however, showed that cryogenic temperature had little effect on panel strength. The average failure loads for the room-temperature (6 and 8) and cryogenic-temperature (7 and 9) damaged panels were 3575 and 3550 lb, respectively. The strengths of the damaged panels, though, were well below the undamaged panel strengths. Since the test specimens were only two corrugations wide and damage was inflicted in both corrugations, there was no alternative load path. If the panels had been wider, the effect of two damaged corrugations would probably have been less severe. The two repaired panels (4 and 5) had strengths that were essentially equivalent to the undamaged panels. The conclusions drawn from these tests were

(1) A correction factor for the room-temperature combined-load tests run at McAir was unnecessary.

Figure 27.—Damage tolerance compression test specimens.

TABLE V.—PHASE I DAMAGE TOLERANCE COMPRESSION PANEL RESULTS

Specimen number	Damage type	Test temper-ature, °F	Buckling load, lb	Failure load, lb
1	No damage	Room	4700	6100
2	No damage	Room	4600	6060
3	No damage	−423	5000	6750
4	Puncture repair	Room	4500	6700
5	Puncture repair	−423	5500	7260
6	Impact damage	Room	2900	3950
7	↓	−423	2500	3400
8	↓	Room	2200	3200
9	↓	−423	2400	3700

(2) Impact damage had a significant effect on test panel strength.

(3) Repaired test panels maintained the undamaged panel strength.

Phase II of the damage tolerance tests consisted of damaged test panels loaded by a combination of compression and shear. These tests were performed by using the McAir test machine described earlier in the section McDonnell Douglas Aircraft (McAir) G-Prime Combined Compression/Shear Load Tests.

Panels similar to those shown in figure 21 were subjected to several types of damage and repairs and then were fatigue tested by using a combined load spectrum gleaned from launch dynamic loads analyses. Tables VI and VII represent the loading spectra used for fatigue testing the forward and aft adapter panels, respectively. Each load spectrum was applied eight times to account for one launch/abort followed by a second launch including a factor of safety of 4. The minimum shear test loads for all steps in both loading spectra were less than zero, and thus provided shear load ranges that were more severe than predicted launch environment conditions. This was necessary because of a peculiarity inherent in the McAir test machine. Unless each shear load cycle was reversed to a value of −5 percent of maximum shear, the maximum shear load would gradually increase from the desired input value. Original calculated load ranges and adjusted load ranges for the forward and aft adapters are shown in tables VI and VII.

TABLE VI.—FORWARD ADAPTER CYCLIC FATIGUE LOADS

Step number	Number of cycles	Compression, lb		Shear, lb	
		Minimum	Maximum	Minimum	Maximum
Calculated loads					
1	2	0	5090	0	4970
2	3	730	4210	711	4110
3	10	1570	4360	1540	4260
4	30	3180	3660	3110	3580
5	30	3750	4210	3660	4110
6	60	4210	4700	4110	4600
7	175	3100	3570	3030	3490
8	125	3460	4210	3380	4110
9	100	3750	4770	3660	4660
10	250	4530	5020	4430	4900
Calculated loads with adjusted minimum shear load for McAir damage tolerance test					
1	2	0	5170	−260	5260
2	3	740	4280	−220	4350
3	10	1600	4430	−230	4510
4	30	3230	3720	−190	3790
5	155	3800	4280	−220	4350
6	60	4280	4770	−250	4860
7	175	3150	3630	−190	3690
8	100	4370	4850	−250	4930
9	250	4600	5090	−260	5180

TABLE VII.—AFT ADAPTER CYCLIC FATIGUE LOADS

Step number	Number of cycles	Compression, lb		Shear, lb	
		Minimum	Maximum	Minimum	Maximum
Calculated loads					
1	1	0	29 890	0	24 120
2	10	2 773	23 310	2 240	18 830
3	30	18 670	21 490	15 080	17 360
4	30	21 940	24 740	17 710	19 980
5	60	24 740	27 540	19 980	22 250
6	175	18 200	21 010	14 690	16 970
7	125	21 940	24 740	17 710	19 980
8	100	25 220	28 030	20 360	22 630
9	250	26 620	29 400	21 500	23 740
Calculated loads with adjusted minimum shear load for McAir damage tolerance test					
1	1	0	29 890	−1200	24 120
2	10	2 773	23 310	−940	18 830
3	30	18 670	21 490	−870	17 360
4	30	21 940	24 740	−1000	19 980
5	60	24 740	27 540	−1110	22 250
6	175	18 200	21 010	−850	16 970
7	125	21 940	24 740	−1000	19 980
8	100	25 220	28 030	−1130	22 630
9	250	26 620	29 400	−1190	23 740

The test procedure was to ultrasonically inspect the panels prior to fatigue testing to establish a baseline for damage size. After fatigue testing, the panels were again ultrasonically inspected to see if the damaged areas had grown. The panels were then statically tested in accordance with their respective design load curves (figs. 14 and 15) to determine whether the damage and fatigue loading had reduced their strength below the required acceptable level.

Table VIII summarizes the results of the McAir damage tolerance testing. The letters associated with each panel number signify whether the test specimen represented the forward adapter (FA) or the aft adapter (AA). The damage configuration describes the amount and type of damage inflicted on the panel. A poorly drilled hole represents a hole with broken fibers on the exit side of the drilled hole caused by a dull drill and excessive pressure. The backside (BS) radius of the panel is the 0.320-in. radius shown in section A-A of figure 2 and in section B-B of figure 5. The front side (FS) flat is the flat surface joining the fillets opposite the 0.320-in. radii. The failure load is the static combined load at which the specimen failed after being subjected to the fatigue loading. The relationship of the failure loads with respect to the ultimate design envelopes is shown in figures 28 and 29. Figure 28 shows that the failure loads for both damaged and undamaged forward adapter panels exceeded the ultimate design envelope. On the basis of this data, it was concluded that a forward adapter with invisible damage would sustain ultimate design

TABLE VIII.—PHASE II McAIR DAMAGE TOLERANCE TEST RESULTS

Panel number	Damage configuration[a]	Failure load, lb/in.	
		Axial	Shear
FA3	Poorly drilled 0.25-in. hole, 4.5 ft-lb impact (BS radius), 1.5 ft-lb impact (FS flat), and resin-rich insert	---	571
FA4	Poorly drilled 0.25-in. hole, 4.5 ft-lb impact (BS radius), and 1.5 ft-lb impact (FS flat)	421	583
FA5	Poorly drilled 0.25-in. hole, 4.5 ft-lb impact (BS radius), 1.5 ft-lb impact (FS flat), and 7-in. Teflon insert with repair patch	474	709
AA7	Poorly drilled 0.25-in. hole, 5 ft-lb impact (BS radius), puncture with repair patch, and delamination between tape and cloth at edge[b]	1573	1510
AA8	Two 5 ft-lb impacts (BS radius and FS flat), and puncture with repair patch	[c]1475	[c]1387
AA9	One 5 ft-lb impact (BS radius), 1.875 ft-lb impact (FS flat), and puncture with repair patch	[d]1544	1044

[a]BS, back side; FS, front side.

[b]Delamination was not intended as part of original damage configuration but was an accident that occurred during panel insertion to test fixture.

[c]AA8 saw greater compression and shear loads at a previous fatigue cycle (1573-lb/in. compression and 1507-lb/in. shear).

[d]AA9 saw greater compression load during previous fatigue cycling and static testing (1798-lb/in. compression with 914-lb/in. shear).

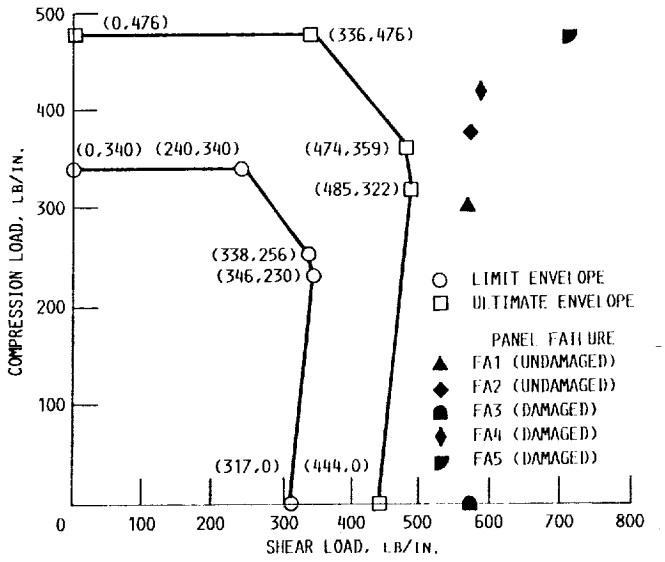

Figure 28.—Static failure loads for G-Prime McAir forward test panels.

loads without premature failure. The forward adapter design contained a large ultimate margin of safety so that the presence of some damage was tolerable.

The aft adapter damaged specimen failed at a combined static load which was less than that prescribed by the ultimate design load envelope, as shown in figure 29. The design margin of safety for the aft adapter was approximately one-half that of

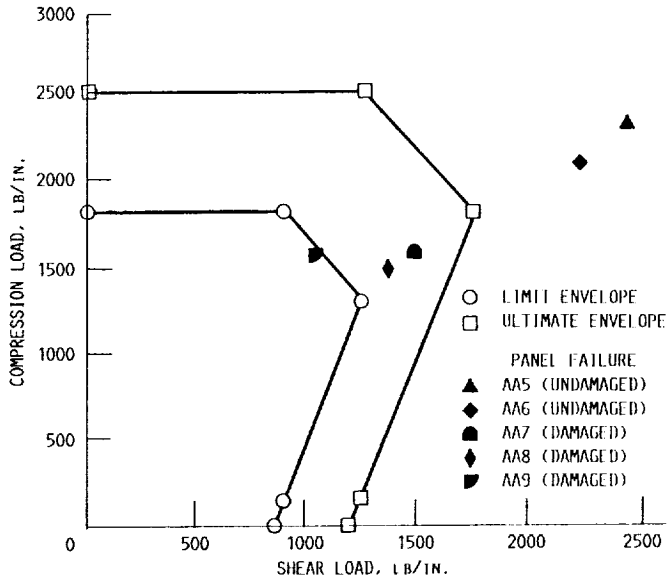

Figure 29.—Static failure loads for G-Prime McAir aft test panels.

the forward adapter so that it was less likely that a damaged aft adapter would sustain ultimate design load without premature failure. Results of the aft adapter damage tolerance tests prompted additional protective measures to be implemented during handling and shipping of the adapter.

G Vehicle Forward Adapter 22-Hardpoint Subcomponent Tests

The G vehicle forward adapter design maintained the same basic structural design as that of the G-Prime vehicle except that 22 hardpoints were provided on the composite section and 8 hardpoints on the forward end of the conical section for mounting optional payload trusses. (The 22-hardpoint truss is shown in fig. 9.) The introduction of concentrated loads into the composite section made it necessary to conduct several subcomponent tests to verify the hardpoint design. Table II lists the basic shell laminate properties for the G and G-Prime vehicles. The G vehicle layup included 45° plies in place of 55° plies to provide additional shear capability. Figure 30 shows a typical composite section hardpoint. The subcomponent tests discussed in the following paragraphs are primarily concerned with the integrity of this design.

Coupon tests.—The original approach to the G vehicle forward adapter stress analysis was to develop laminate strength and stiffness properties by using a standard laminate properties computer code. This code had been used to correctly reproduce test results for the G-Prime vehicle laminates ($[55/125/0/90]_s$), so it was assumed that the code would provide reliable properties for the G vehicle layup ($[0/\pm 45/0/90/0]_s$). However, as an added precaution, it was decided to perform a limited number of coupon tests to substantiate the theoretical values. The tests included room-temperature and cryogenic tension tests, room-temperature in-plane shear and short-beam shear tests, and

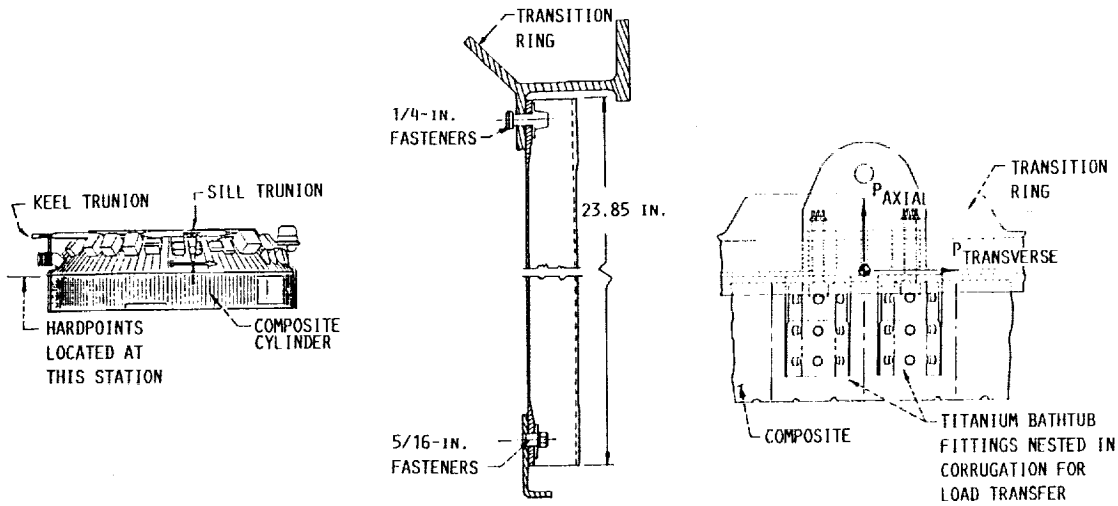

Figure 30.—G vehicle forward adapter 22-hardpoint design (0.06-in. base laminate, 0.203-in. maximum buildup, 25 hardpoint attachments (22 payload truss, 2 sill drag strut, 1 keel drag strut)).

TABLE IX.—G FORWARD ADAPTER COUPON TEST RESULTS
[Materials are T300/934 tape and T300/934 cloth.]

Test type (flat coupon)	Laminate[a]	Temperature, °F	Specimen number	Average thickness, in.	Analysis thickness (ref.), in.	Average stress, ksi	Standard deviation, ksi	Coefficient of variation
Tension	A	Room	10	0.064	0.060	119.4	3.55	0.03
		−423	10	.065		71.1	7.10	.10
In-plane shear		Room	6	.063		36.3	1.19	.03
Short-beam shear		Room		.064		14.9	.922	.06
1/4-in. fastener	B	−423, −320		.174	.164	101.8	2.12	.02
5/16-in. fastener	C	−423, −320		.214	.203	75.8	1.82	.02

[a]Laminates A, B, and C are defined as follows: A, $[0/\pm 45/0/90/0]_s$ tape base; B, base + $[45/0_2/45]_s$ cloth; C, base + $[45/0_2/45_2/0_2/45_2 0/45]$ cloth.

TABLE X.—COMPARISON OF ANALYSIS AND TEST RESULTS

Test type (flat coupon)	Jones technique[a]			Analysis A allowable	Test average/ analysis A	Test A/ analysis A strength[b]	Test modulus	Standard deviation	Analysis modulus, msi	Test modulus/ analysis modulus stiffness[b]
	Coefficient of variation	γ	A allowable, ksi							
Tension										
Room temperature	0.10	0.82	97.8	77.4	1.54	1.26	11.5	0.098	12.1	0.95
Cryogenic temperature	.10	.82	58.3	53.1	1.22	1.00	12.3	.161	12.1	1.02
In-plane shear	.06	.87	31.6	28.7	1.26	1.10	----	-----	2.24	----
Short-beam shear	.06	.87	13.6	Not used	----	----	----	-----	----	----
1/4-in. fastener	.10	.81	82.5	64.0	1.59	1.29	----	-----	----	----
5/16-in. fastener	.10	.81	61.4	73.0	1.04	.84	----	-----	----	----

[a]See reference 1.
[b]Shows degree to which tests validated assumed values (≥ 1.0 desired).

cryogenic fastener bearing tests. Tables IX and X summarize the test results. Table IX lists the number of specimens and the average failure stress for the various coupon tests. Table X compares the A allowables derived from the test data by using the Jones technique (ref. 1) and the values obtained from the laminate properties computer code. The values in the columns headed "Test A/analysis A strength" and "Test modulus/analysis modulus stiffness" represent the ratio of the test value and the analysis value. A ratio of 1 signifies exact agreement between the analytical and test values.

The room-temperature statistical A-basis tensile allowable was 26 percent higher than the analysis allowable, and the test modulus was 5 percent lower than the analysis modulus. The small difference in the modulus had little effect on the adapter stress analysis, and the use of the analytical allowable produced adapter analysis results that were conservative. The test cryogenic-temperature strength and stiffness values compared rather well with the analytical values (ratios of 1.00 and 1.02, respectively). There was a notable reduction between the room-temperature and cryogenic-temperature strength values. This was accounted for in the adapter stress analyses.

The room-temperature in-plane shear A-basis test value was 10 percent greater than the A-basis analysis allowable. The A-basis test value matched the A-basis allowable exactly when shear strains only were considered. However, the calculated design allowable considered tensile strains in the 45° plies which occur when shear is applied to the laminate. This resulted in a design allowable that was 10 percent lower than the A-basis test value.

The short-beam shear test is not suitable for the generation of design allowables, but it does provide a means to measure laminate compaction quality. The test data were used to establish an acceptance value for short-beam shear tests performed on tag end specimens acquired from production panels. The average room-temperature test value was used to signal a degradation in production quality.

The 1/4-in.- and 5/16-in.-diameter fastener tests were performed to investigate the difference in composite bearing strength at LN_2 (−320 °F) and LH_2 (−423 °F) temperature. This was necessary because the three-fastener subcomponent tests, which are discussed in the next subsection, could not be performed at the LH_2 temperature environment expected for the shuttle/Centaur in the fastener region. It was necessary to determine the difference so that an appropriate compensating factor, if required, could be applied to the three-fastener tests.

The 1/4-in. fastener specimens were 0.174 in. thick, representing the built-up area, and 1.75 in. wide. One 0.25-in. hole was placed midwidth at each end with a 0.5-in. edge distance from the specimen end. Test results showed that total failure occurred when the average bearing stress (load/(diam × thickness)) reached 102 ksi for both the LH_2 and LN_2 test temperatures. The actual failure mode was cleavage/net tension so that the bearing stress is a reference value only. (A cleavage/net tension failure can be described as a combination of a net section tensile failure and a shear tear-out failure.) It was originally thought that fastener bearing would be critical, but the tests produced results that were well beyond those expected. The A-basis test allowable of 82.5 ksi was 29 percent higher than the 64.0-ksi analysis allowable.

The 5/16-in. fastener specimens were similar to the 1/4-in. fastener specimens except that the thickness was 0.214 in. and the fastener holes were 5/16 in. in diameter. This represented the aft ring area laminate buildup in special areas where closely spaced hardpoints resulted in load overlap at the aft ring joint. Although the larger fastener provided more bearing area, the cleavage/net tension failure mode was dominant. Because the edge distance was maintained at 0.5 in. for the 5/16-in. fastener, the cleavage strength was less than that for the 1/4-in. fastener even though the buildup thickness was larger. The average fastener bearing stress was 75.8 ksi when cleavage failure occurred. Although the reference bearing strength was less than anticipated, evaluation of the margin of safety for the 5/16-in. bolt applications showed the strength to be adequate. Once again the values obtained at LN_2 and LH_2 temperatures were essentially the same so that no compensating factor was required for the three-fastener subcomponent tests that follow.

Three-fastener subcomponent tests.—The purpose of the three-fastener tests was to assure that the required axial load could be safely introduced through fasteners into the tape/cloth edge built-up region of the G vehicle forward adapters, and then pass through ply dropoffs to the base tape layup of the panel. The specimens consisted of corrugated graphite/epoxy panels representative of selected areas of the G vehicle forward adapter. There were two test panel types (types I and II), each three corrugations wide, as shown in figures 31 and 32, respectively.

Three type I specimens were tested. They represented the base laminate ($[0/\pm45/0/90/0]_s$) plus the cloth buildup ($45/0_2/45_2/0_2/45_2/0/45$) in the region of the 5/16-in. ring fasteners for a total thickness of 0.203 in. The 5/16-in. fasteners were used selectively in aft ring regions where load overlap from closely spaced hardpoints required additional strength.

Three type II specimens were also tested. Each specimen end represented the base laminate ($[0/\pm45/0/90/0]_s$) plus the cloth buildup ($45/0_2/45/45/0_2/45$) in the aft ring region in line with a typical payload hardpoint, making the total thickness 0.164 in. in this region.

The test plan for the three-fastener subcomponent tests is given in the appendix. A conservative approach was used to establish test loads. It was assumed that each hardpoint was subjected to 15 400 lb ultimate axial load and 8000 lb ultimate shear load, simultaneously. Stress analysis showed that, in the area where a hardpoint was near a sill drag link attachment, the ultimate bolt loads were 3754 lb axial and 1545 lb shear. The shear load could not be introduced into the test specimen, so it was conservatively included with the axial load by vectorally summing the two loads. This produced a resultant total load of 12 180 lb for the three fasteners of the type I specimen.

The type II specimens represented the laminate buildup and ply dropoffs in the aft ring region in line with a typical hardpoint where no load overlap occurred and 1/4-in. fasteners were adequate. The calculated ultimate bolt loads were 2193 lb axial and 1332 lb shear, which gave a resultant total load of 7700 lbs for the three fasteners of the type II specimen.

The fatigue loading was obtained from shuttle/Centaur dynamic analysis spectrum data. The highest g load was taken to be limit load. The spectrum loads were ratioed to the limit load according to the ratio of their corresponding g loads and

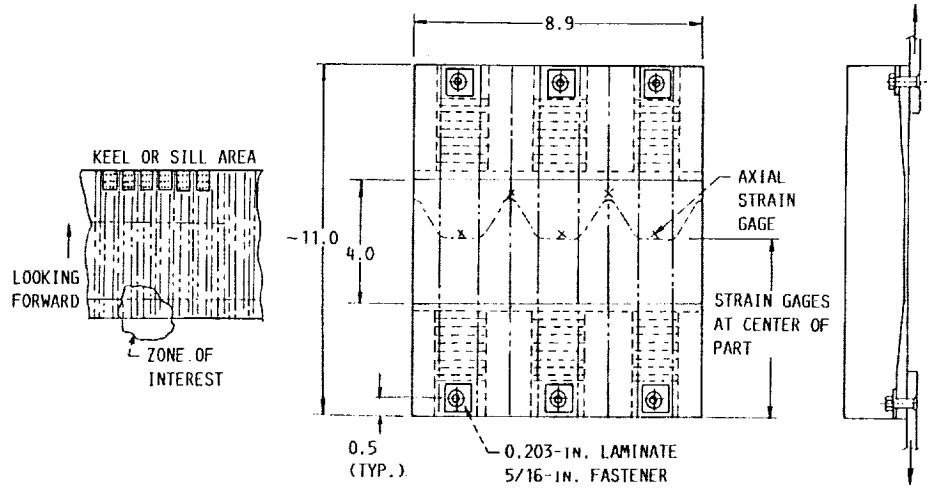

(b)

(a) Specimen.
(b) Schematic (dimensions in inches).

Figure 31.—Type I aft ring fastener tensile specimen and schematic.

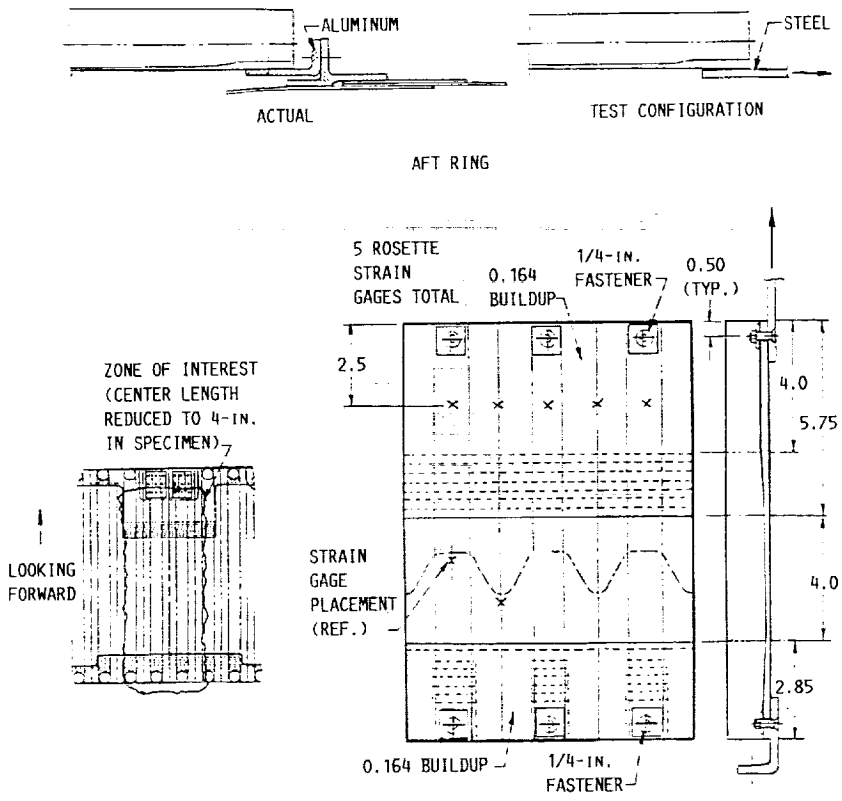

Figure 32.—Type II hardpoint ply dropoff tensile specimen schematic (dimensions in inches).

the maximum g load. Loads that were less than 50 percent of the ultimate load were not considered. After reviewing the spectrum data, it was decided to take the conservative approach and cycle the specimens between limit tension and limit compression ($R = -1.0$) because the bulk of the loads were within 84 to 95 percent of the limit load. The total number of cycles for these loads was 566. Applying the standard factor of 4 for life estimates and an additional factor of 2 to account for an abort landing and subsequent lift-off, the total number of test cycles was determined as 4600. Thus type I and type II specimens were subjected to 4600 cycles of ± 8700 and ± 5500 lb, respectively (ultimate bolt load divided by 1.4).

The three type I specimens met all of the test plan requirements with no sign of damage. The average failure load of 14 875 lb was 22 percent higher than the expected ultimate load of 12 180 lb. The failure mode was similar to the cleavage/net tension failure experienced by the 5/16-in. fastener flat coupons discussed in the subsection Coupon Tests. The average failure load of 4958 lb/fastener (14 875 lb/3 fasteners) for the three-fastener specimens was within 3 percent of the average failure load of the flat coupons. The cryogenic fatigue portion of the test apparently did not affect the fastener failure mode. Interlaminar shear in the ply dropoffs was not a problem.

Each of the three type II specimens also met all the test plan requirements with no sign of damage. The average failure load of 13 017 lb was 69 percent higher than the expected ultimate load of 7700 lb. The failure mode was typical of the type experienced by the other fastener specimens. The average failure load per fastener of 4339 lb was again within 3 percent of the average failure load of the corresponding flat coupons indicating that the cryogenic fatigue cycles had no effect on the fastener failure mode. There was no visible indication that interlaminar shear in the ply dropoffs would be a problem.

Short-beam hardpoint subcomponent tests.—Figure 33 shows the short-beam hardpoint test specimen. This specimen was designed to verify the local strength of a typical payload hardpoint subjected to biaxial loading. The specimen was symmetrical to allow proper load introduction—thus two hardpoints per specimen were tested. Axial and shear loads were applied through fittings on each end of the specimen and a load strap at the specimen midpoint. The corrugations under the load strap were reinforced to prevent crushing when shear load was applied. The titanium fittings and composite buildup were representative of the actual hardware. Three specimens were built and tested. The first specimen was tested according to the test plan given in the appendix to the loads shown in figure 34. The other two specimens were tested to a slightly different load diagram, as shown in figure 35, using the same test plan procedure. The load envelopes were squared off for these specimens and created a more severe loading condition.

Testing of the first specimen began with the room-temperature limit load survey. Analysis of the specimen strain gage readings verified that the specimen was loaded correctly.

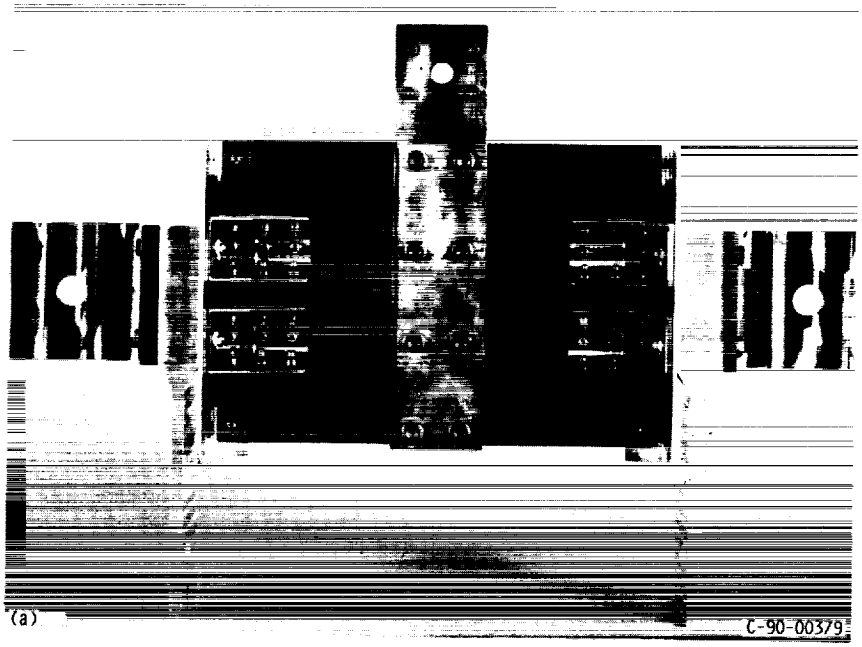

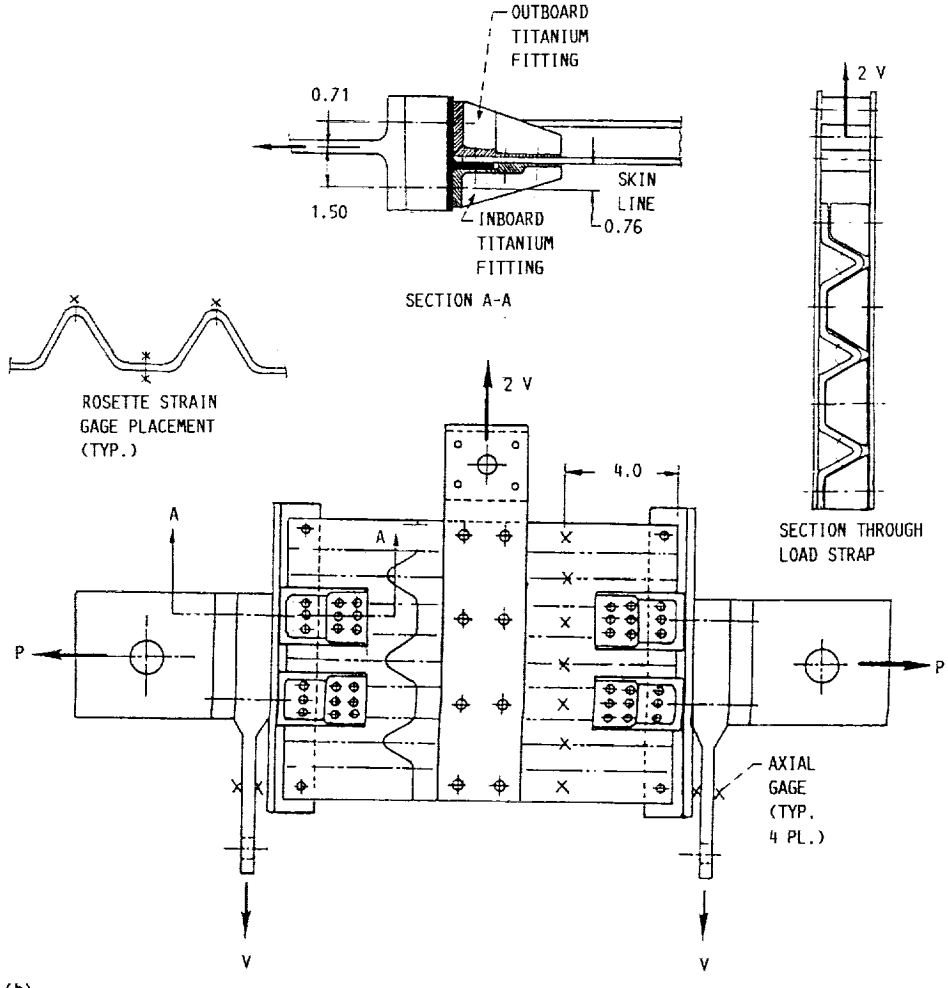

(a) Specimen.
(b) Schematic.

Figure 33.—Short-beam hardpoint combined load test specimen and schematic (dimensions in inches).

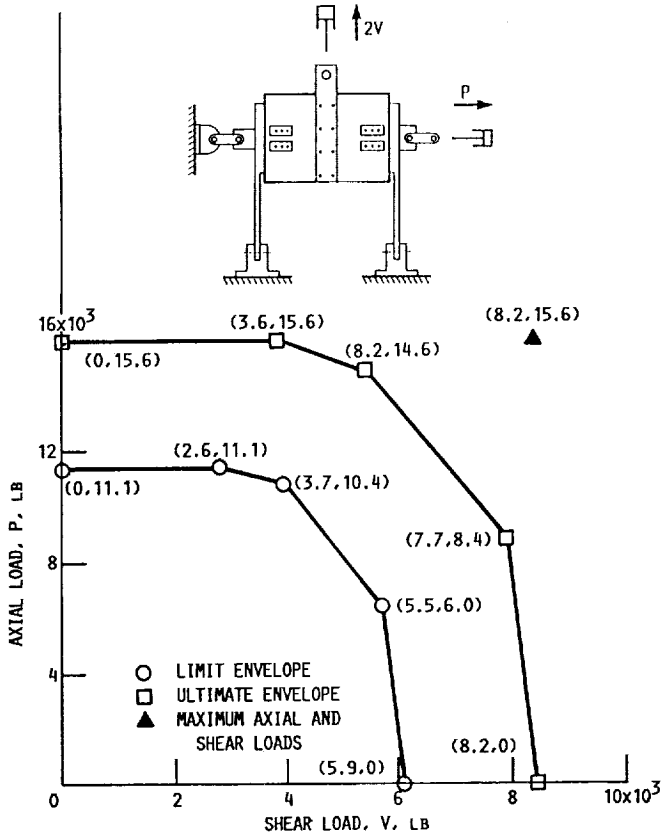

Figure 34.—Short-beam test load diagram and schematic.

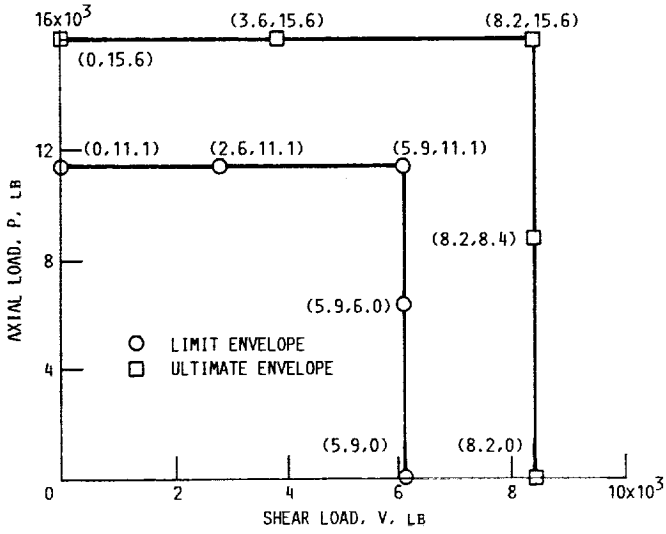

Figure 35.—Short-beam test revised load diagram.

Load points were then repeated at −65 °F, which was the expected flight temperature. The purpose of this test was to introduce thermal loads caused by the difference in coefficient of thermal expansion between the graphite/epoxy and the titanium fittings. Fatigue testing at −65 °F followed the low-temperature limit load survey. The specimen was cycled 4600 times by applying a 11 100 lb axial load and 5200 lb total shear load, simultaneously at $R = 0.1$. Visual examination after the fatigue test showed no damage.

Next, the specimen was subjected to ultimate loads at room temperature and then at −65 °F. Nothing unusual occurred during these tests.

During the earlier limit load test at −65 °F, a load cell failure caused the specimen to be accidentally loaded to 29 900 lb tension (1.94 times ultimate axial load) without failure. Therefore, it was decided to alter the test plan slightly, and the specimen was loaded to 15 600-lb ultimate axial load P and 8200-lb ultimate shear load V. (See fig. 34.) The specimen withstood this load, so combined axial and shear loading was increased along a path defined by a straight line through this point and the origin. Load application was halted at 157 percent of ultimate ($P = 24\ 500$ lb, $V = 12\ 900$ lb). The specimen was visually inspected, and no damage other than some yielding of the closed end of the outboard titanium fitting was observed. The thickness of this end pad was smaller (0.180 in.) than that specified for the flight hardware (0.230 in.).

Because the load-carrying capability of the first specimen was higher than expected, the remaining two specimens were subjected to a more severe test by squaring off the load envelopes, as shown in figure 35. Both specimens survived all the tests required by the test plan using the increased load diagrams. Testing of one of the specimens was halted at 157 percent of biaxial ultimate as was done for the first specimen. Post-test visual inspection revealed no sign of impending failure. The remaining specimen was loaded beyond the 157 percent ultimate load along a line through this point and the origin. Failure occurred at 171 percent of ultimate ($P = 26\ 700$ lb, $V = 14\ 000$ lb).

On the basis of these tests, it was concluded that the load-carrying capability of the G vehicle hardpoints was more than adequate for the expected axial/shear/temperature loads. Furthermore, limit load fatigue cycling appeared to have no harmful effect.

Full-panel hardpoint test.—The objective of the full-panel hardpoint test was to verify that a concentrated axial load through a hardpoint could be safely dispersed through ply dropoffs into the basic laminate. Figures 36 and 37 show the full hardpoint test specimen. The specimen was approximately 25 in. high, which was the actual height of the forward adapter, and seven corrugations wide (approximately 22 in.). Aluminum angles were included at both ends to represent the adapter forward and aft attachment rings. The specimen vertical edges were reinforced with graphite/epoxy cloth to prevent free-edge buckling. The lower end of the specimen was immersed in liquid nitrogen (fig. 37) to account for aft ring contraction when cryogenic propellants are loaded on the vehicle and to account for material low-temperature properties. Strain gages were located at various locations on the panel to assure proper load introduction to the panel.

The test plan for the full-panel subcomponent test is given in the appendix. Strain gage data showed that the actual load dispersion from the hardpoint to the most highly loaded aft

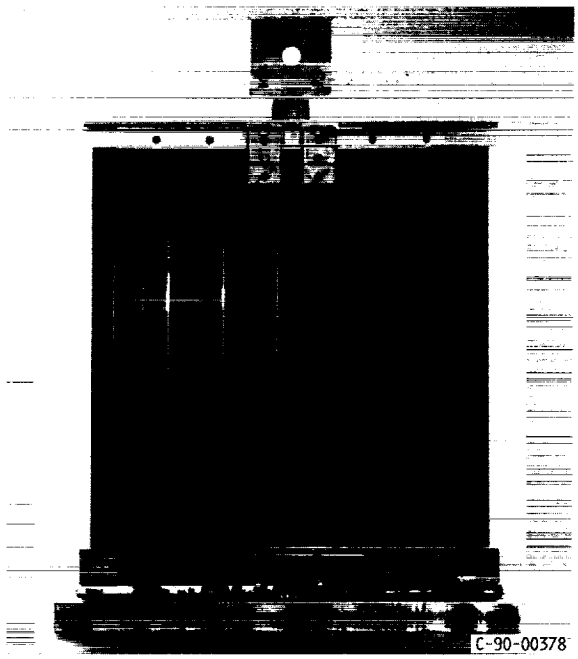

Figure 36.—G vehicle forward adapter panel with hardpoint (backside).

ring fastener agreed well with that assumed for fastener analyses (14.5 percent compared to the assumed value of 14.0 percent). During the initial design of the G vehicle forward adapter, a considerable analytical effort was made to characterize load dispersion. Results were quite sensitive to model configuration so that it was difficult to establish confidence in the predicted load dispersion pattern. The stiffness of the forward transition ring and the number of corrugations in the model greatly influenced the dispersion pattern. The simulated transition ring on the test specimen was purposely not as stiff as the production hardware in order to provide a more conservative evaluation of the hardpoint test panel.

As noted in the test plan given in the appendix, the highest planned test load in tension and compression was 19 400 lb. In the actual test, the highest load in tension was 19 502 lb (127 percent ultimate), and the highest compression load was −25 054 lb (163 percent ultimate). The panel did not fail. The fact that the panel sustained loads in excess of ultimate without failure was not totally unexpected. The design verification coupon and short-beam hardpoint tests discussed earlier showed excess strength in various portions of the design. The full-panel test was the first test that compiled the various features of the previous hardpoint subcomponent tests to establish the integrity of the design. The test did not include the hardpoint shear force so that excess load capacity beyond ultimate was necessary to assure that the adapter would be capable of carrying combined loads.

Full-Scale Vehicle Structural Test

The full-scale G-Prime vehicle structural test was performed at the General Dynamics Sycamore Canyon Test Site. A dedicated test vehicle (fig. 38) which resembled the flight vehicle as much as possible was statically load tested. Figure 39 shows the various vehicle loading points. The various loads and their functions are listed in table XI.

Five strain gages were mounted on the forward adapter composite section and seven on the aft adapter. These gages were mounted in the flat sections of the corrugations at various locations around the periphery of the adapters. Their purpose

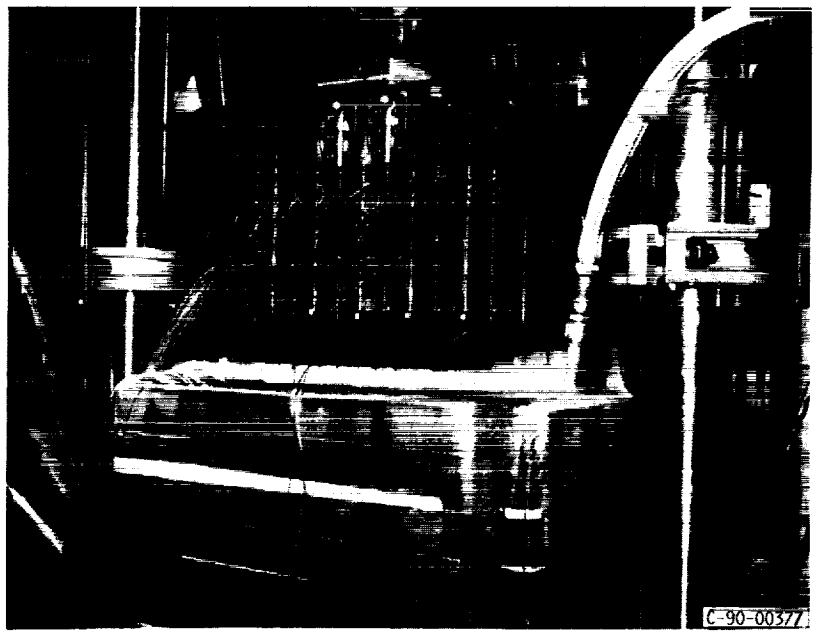

Figure 37.—G vehicle hardpoint test panel with aft end in LN_2 bath.

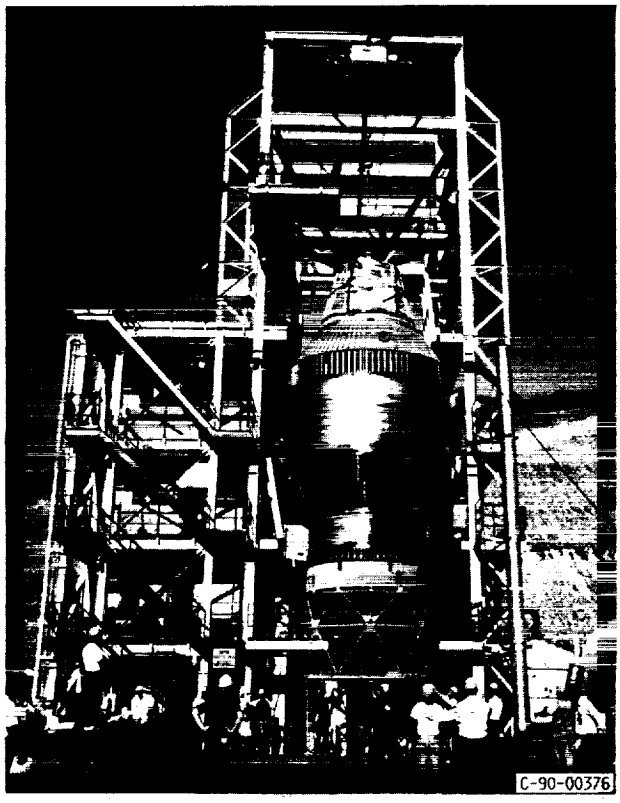

Figure 38.—G-Prime test vehicle being installed in test stand.

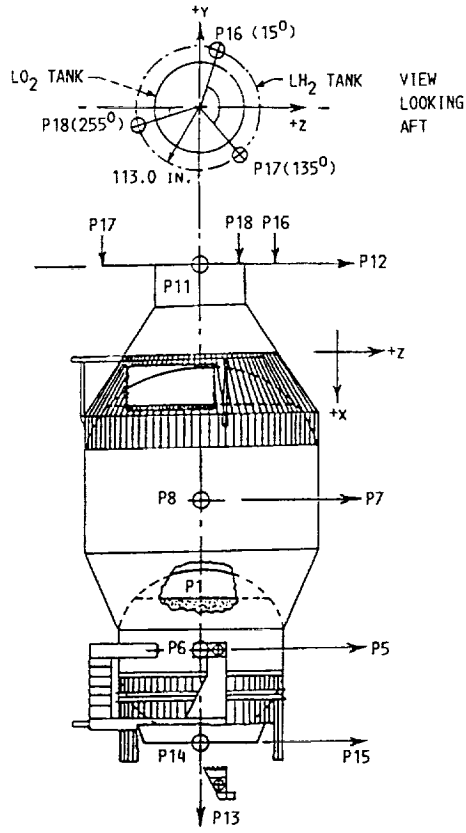

Figure 39.—Full-scale G-Prime vehicle structural test configuration (positive loads applied in directions $+x$, $+y$, and $+z$).

was to compare the test strain values to those predicted by the analysis models. Figures 40 and 41 are comparisons of the measured strains and the predicted strains for the forward and aft adapters, respectively. The measured strains are from a test load case that had loads applied to all load points. The loads applied at each point are listed in table XI. The LO_2 tank was loaded with liquid nitrogen at 45 psig and the LH_2 tank with liquid hydrogen at 31 psig. The applied loads provided a loading condition that was 20 percent higher than the design loads.

Figure 40 shows a comparison of the measured and theoretical axial strains for the forward adapter. The continuous line represents the theoretical axial strain predicted by the NASTRAN model at various circumferential locations. The double bars at each location represent a test-measured axial strain and an axial strain that was corrected for the bending that resulted from the corrugations. The NASTRAN model did not model the corrugations but used plate elements with orthogonal properties to account for the biaxial stiffness of the corrugated structure. Consequently, the NASTRAN model could not account for the bending component, so the measured strain had to be corrected to eliminate the bending strain included in the measured strain. The angular locations in figure 40 are referenced to the 0° axis shown in figure 39.

The corrected measured strains compared well with the predicted strains at three of the five locations shown in figure 40. The corrected measured value at 12° was larger than predicted, but the other four were smaller and agreed fairly well with the predicted value except for the 48° location. The gage at the 12° location was near the point where a forward support drag link attached to the composite adapter, and the gage at the 48° location was in the vicinity of the pneumatic line cutouts. This could account for the discrepancy between the corrected measured values and the predicted values because of the complex stress field in these areas.

TABLE XI.—FULL-SCALE G-PRIME VEHICLE STRUCTURAL TEST LOADS

Loading point	Function	Load, lb
P5	LO_2 propellant lateral inertia load	150 000
P6	LO_2 propellant lateral inertia load	75 000
P7	LH_2 propellant lateral inertia load	7 100
P8	LH_2 propellant lateral inertia load	11 700
P11	Spacecraft lateral load	−11 500
P12	Spacecraft lateral load	−23 100
P13	LO_2 propellant longitudinal inertia load	145 000
P14	Engine gimbal lateral load	8 000
P15	Engine gimbal lateral load	8 000
P16	Spacecraft longitudinal load	20 100
P17	Spacecraft longitudinal load	1 100
P18	Spacecraft longitudinal load	15 200

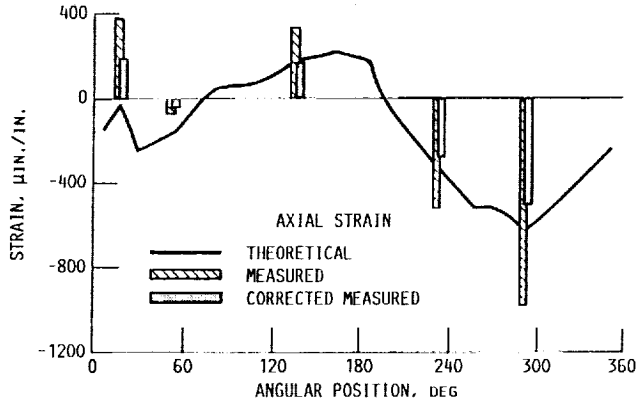

Figure 40.—Comparison of measured and theoretical axial strains for forward adapter.

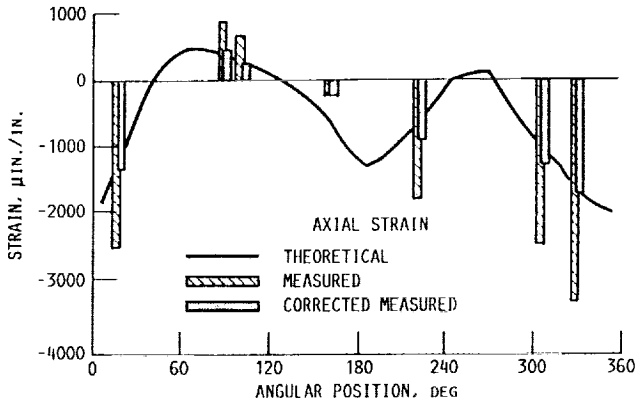

Figure 41.—Comparison of measured and theoretical axial strains for aft adapter.

Figure 41 shows the aft adapter measured and theoretical strains for the same load case applied to the forward adapter. The zero angle reference is the same, and the double bars represent a measured and corrected value as before. The corrected measured strain values agreed well with the theoretical values except at the 160° location, which was in the vicinity of the LO_2 vent and instrumentation cutouts. The complex stress field near the cutouts could again explain the discrepancy.

The good correlation between the corrected measured strains and the theoretical strains provided confidence in the NASTRAN model at the adapter locations. Consequently, all loads used for the subcomponent tests discussed earlier in this section were valid, and the adapters were judged as acceptable flight components.

Concluding Remarks

Application of graphite/epoxy to primary structure for the shuttle/Centaur program involved a number of unprecedented challenges. The corrugated composite adapters proved to be workable and met requirements for a manned launch. Use of graphite/epoxy at cryogenic temperatures as well as other issues required an extensive evaluation program to certify the designs for flight. Analysis played a significant role in the design process, but all critical regions of the adapters were thoroughly tested at the subcomponent level. In addition, the production panels included large "tag end" segments which were cut into a number of specimens to verify panel integrity.

Most design verification tests demonstrated more-than-adequate strength. Part of this excess strength was due to the use of statistical design allowables, but the entire design process itself had proceeded in a conservative manner since a great deal was at stake with this new technology. Strong interaction and cooperation between NASA and General Dynamics Space Systems Division assured a successful program.

The damage tolerance tests showed that the G-Prime vehicle aft adapter was more sensitive to damage than the forward adapter. The aft adapter loads were much higher and the design margin was smaller. Invisible damage, which was impossible to detect once the panels were assembled, was particularly critical in reducing the aft adapter strength to a level below the ultimate design load. Therefore, it was necessary to take special precautions to protect the aft adapter from damage by providing protective covers. Protective covers for the forward adapter were also provided as an added precaution.

Proof testing the completed adapters before assembly to the vehicle was impractical because of their size and the large combined axial and shear load required. In addition, there was always some doubt about the extent of damage that could be introduced during the proof test. Inspection following proof testing is desirable but impractical unless a reliable portable method can be employed.

The corrugated design provided good axial strength but was inherently weak in shear near the end regions. The overturning moment created by the shear flow through the corrugations introduced a bending moment in the radius between the corrugation flat and the inclined surface and a tearing force at the fasteners. The corner radii were particularly susceptible to voids due to layup and compaction difficulties, thereby creating weak spots. Rectangular washers were used under the fastener heads to increase bearing area and to decrease the tearing action aggravated by round washers.

Although the space shuttle/Centaur G-Prime and G vehicle programs were discontinued, a modified G-Prime vehicle is in progress for launch by a Titan IV vehicle. The basic configuration has been maintained except that the aft adapter is no longer made of graphite/epoxy. An aluminum skin/stringer design has replaced the corrugated composite. The forward adapter configuration is basically the same except that additional plies have been added to accommodate the higher loading conditions imposed by the Titan. Also the G vehicle 22-hardpoint capability has been incorporated.

Lewis Research Center
National Aeronautics and Space Administration
Cleveland, Ohio, December 11, 1989

Appendix—Subcomponent Test Procedures

Fastener Buildup Subcomponent Test Plan

The following is a step-by-step listing of the fastener buildup subcomponent test plan for the G vehicle forward adapter. Tests were performed at room temperature and at −320 °F for type I and type II panels. (See sketch.)

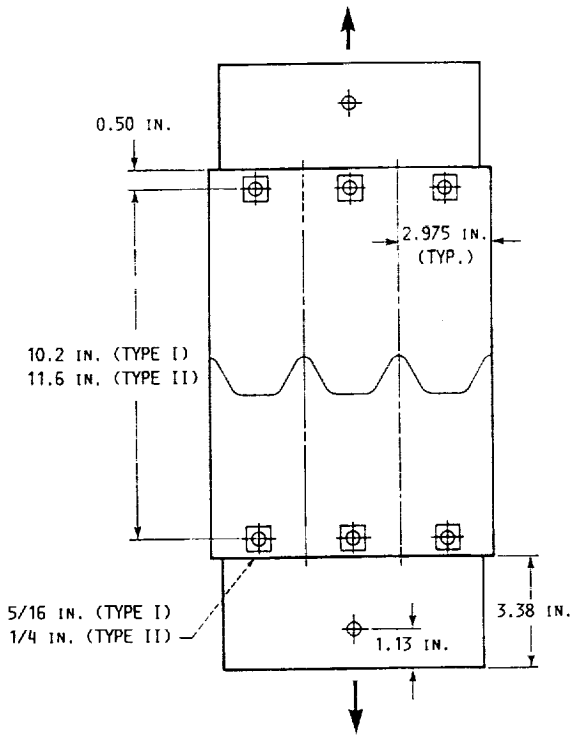

(1) At room temperature, apply tension load (8700 lb for type I and 5500 lb for type II) and hold for 10 sec. Record strain gage data in 10 percent load steps.

(2) Repeat step 1 with compression load (−8700 lb for type I and −5500 lb for type II).

(3) Repeat step 1 at −320 °F.

(4) Repeat step 2 at −320 °F.

(5) At −320 °F, apply 4600 cycles of fatigue at $R = -1.0$ at 0.5 cycles/sec (tension load, 8700 lb for type I and 5500 lb for type II; compression load, −8700 lb for type I and −5500 lb for type II).

(6) Warm and remove specimen from test machine. Examine composite attachments for signs of elongation. Visually examine ply dropoffs for signs of delaminations. Remove center fastener from each end of the specimen and measure hole diameter for signs of elongation. Replace center fasteners and reinstall specimen in test machine.

(7) At −320 °F, apply compression load (−12 180 lb for type I and −7700 lb for type II) and hold for 10 sec. Record strain gage data in 10 percent load steps.

(8) Repeat step 7 with tension load (12 180 lb for type I and 7700 lb for type II).

(9) Continue from step 8, increasing tension load until failure. Record strain gage data.

Short-Beam Hardpoint Subcomponent Test Plan

The following is a step-by-step listing of the short-beam hardpoint subcomponent test plan for the G vehicle forward adapter. Tests were performed for three specimens (see sketch) at room temperature and at −65 °F.

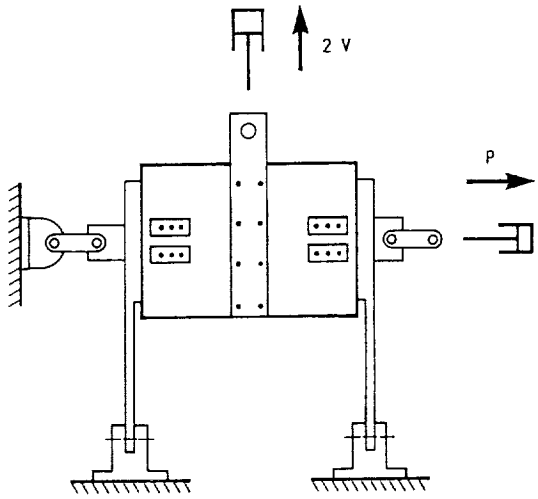

(1) At room temperature, apply limit loads as shown in figure 34. Ramp axial load (P) and twice the shear load ($2V$) simultaneously from zero load for each case. Hold final load 10 sec. Record strain gage data in 10 percent load steps. (For first specimen only, allow 2 days for engineering study of data prior to continuing test.)

(2) Repeat step 1 at −65 ± 10 °F.

(3) At −65 ± 10 °F, apply 4600 cycles of fatigue at $R = 0.1$ using 2600-lb shear load and 11 100-lb axial load. Ramp loads simultaneously.

(4) Halt test, warm to room temperature. Visually examine composite specimen for surface indications of fatigue damage. Photograph any unusual indications. Check strain gage; replace as required.

(5) Repeat step 1 with ultimate load cases, as shown in figure 34.

(6) Repeat step 2 with ultimate load cases.

(7) Halt all testing on one specimen; retain it for engineering disassembly and inspection (no further mechanical loads).

(8) For remaining two specimens, apply 8200-lb shear load and 15 600-lb axial load at −65 °F. Continue ramping P and $2V$ to failure (halt at 220 percent limit to protect fixturing).

Full-Panel Subcomponent Test Plan

The following is a step-by-step listing of the full-panel subcomponent test plan for the G vehicle forward adapter. One specimen was tested. Strain gage data were recorded for all tests, and the test setup was photographed from several angles.

(1) At room temperature, apply 11 000-lb axial tension load and hold for 10 sec. Record strain gage data in 10 percent load steps.

(2) Repeat step 1 with 11 000-lb axial compression load and hold for 10 sec.

(3) Allow 2 days for engineering evaluation of data prior to continuing test.

(4) Repeat steps 1 and 2 with lower 6 in. of panel submerged in LN_2. (See sketch.)

(5) With the lower end still in LN_2, apply 15 400-lb tension load and hold for 10 sec. Record strain gage data in 10 percent load steps.

(6) Repeat step 5 with −15 400-lb compression load.

(7) Continue applying compression to −16 900 lb (110 percent ultimate) and hold for 10 sec minimum. Record strain gage data at 500-lb steps. Return to zero.

(8) With the lower end in LN_2, alternate between tension and compression according to the following schedule. Record data at 8000 lb (or −8000 lb) and at 15 400 lb (or −15 400 lb). Then record data at 500-lb steps beyond 15 400 lb.

(a) Zero to 16 900 lb tension (110 percent ultimate)
(b) Zero to −18 400 lb compression (120 percent ultimate)
(c) Zero to 18 400 lb tension (120 percent ultimate)
(d) Zero to −19 400 lb compression (125 percent ultimate)
(e) Zero to 19 400 lb tension (125 percent ultimate)
(f) Zero to compression to be determined, halt at engineering direction

(9) If panel is intact, test at room temperature to 15 400 lb tension and −15 400 lb compression (100 percent ultimate). Halt testing, return panel to engineering.

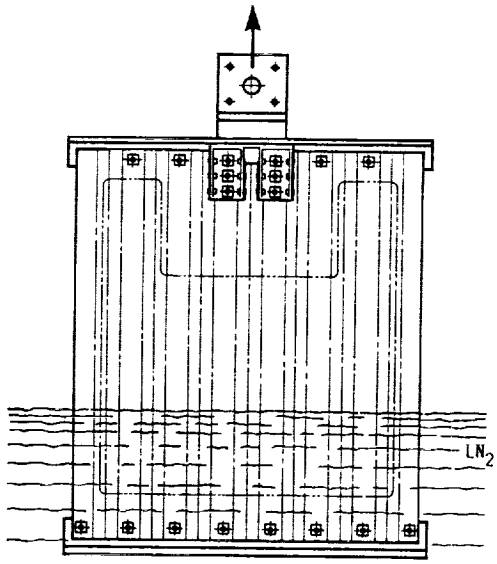

References

1. Jones, B.H.: Determination of Design Allowables for Composite Materials. Composite Materials: Testing and Design, ASTM STP-46O, American Society for Testing and Materials, 1969, pp. 307-320.
2. Ring, D.S.: Centaur G Composite Adapters Stress Report, Vol. 1, Design Criteria. Shuttle/Centaur Report No. CGCA-85-001, General Dynamics Space Systems Div., San Diego, CA, Dec. 1985.
3. Ring, D.S.: Centaur G Composite Adapters Stress Report, Vol. VI, G Forward Adapter Test Results. Shuttle/Centaur Report No. CGCA-85-001, General Dynamics Space Systems Div., San Diego, CA, Dec. 1985.
4. Ring, D.S.: Centaur G Composite Adapters Stress Report, Vol. VI, G Forward Adapter Test Results, Addendum AD-1, Test Report Memos from Test Group. Shuttle/Centaur Report No. CGCA-85-001, General Dynamics Space Systems Div., San Diego, CA, Dec. 1985.
5. Ring, D.S.: Centaur G Composite Adapters Stress Report, Vol. VII, Miscellaneous S/C G Vehicle Composite Stress Memos. Shuttle/Centaur Report No. CGCA-85-001, General Dynamics Space Systems Div., San Diego, CA, Dec. 1985.
6. Sollars, T.A.; and Spier, E.E.: Stability Analysis and Test Verification of Shuttle/Centaur Composite Corrugated Adapters. 26th Structures, Structural Dynamics and Materials Conference, Part 2, AIAA, 1985, pp. 23-30.
7. Cope, K.W.; and Cackett, M.T.: Development of Corrugated Composite Adapters for Shuttle/Centaur. Paper presented at the AIAA 1985 Aerospace Engineering Conference and Show, Los Angeles, CA, Feb. 1985.
8. Sollars, T.A.: Shuttle/Centaur G-Prime Composite Adapters Damage Tolerance/Repair Test Program. 28th Structures, Structural Dynamics and Materials Conference, Part 1, AIAA, 1987, pp. 362-375.
9. Spier, E.E., et al.: Stability Analysis of Centaur-in-Shuttle Composite Corrugated Adapters. 24th Structures, Structural Dynamics and Materials Conference, Part 1, AIAA, 1983, pp. 600-611.

NASA
National Aeronautics and Space Administration

Report Documentation Page

1. Report No.	2. Government Accession No.	3. Recipient's Catalog No.
NASA TP-3014		

4. Title and Subtitle	5. Report Date
Graphite/Epoxy Composite Adapters for the Space Shuttle/Centaur Vehicle	September 1990
	6. Performing Organization Code

7. Author(s)	8. Performing Organization Report No.
Harold J. Kasper and Darryl S. Ring	E-4969
	10. Work Unit No.
	None

9. Performing Organization Name and Address	11. Contract or Grant No.
National Aeronautics and Space Administration Lewis Research Center Cleveland, Ohio 44135-3191	
	13. Type of Report and Period Covered
	Technical Paper

12. Sponsoring Agency Name and Address	14. Sponsoring Agency Code
National Aeronautics and Space Administration Washington, D.C. 20546-0001	

15. Supplementary Notes

Harold J. Kasper, NASA Lewis Research Center; presently at Analex Corporation, NASA Lewis Research Center, Fairview Park, Ohio 44126. Darryl S. Ring, General Dynamics Space Systems Division, San Diego, California 92123 (work funded by NASA Contract NAS3-2290).

16. Abstract

The decision to launch various NASA scientific and Air Force spacecraft from the space shuttle created the need for a high-energy upper stage capable of being deployed from the cargo bay. Two redesigned versions of the Centaur vehicle which employed a graphite/epoxy composite material for the forward and aft adapters were selected. Since this was the first time a graphite/epoxy material was used for Centaur major structural components, the development of the adapters was a major effort. This report includes (1) an overview of the composite adapter designs, (2) results of subcomponent design evaluation tests, and (3) composite adapter test results from a full-scale vehicle structural test.

17. Key Words (Suggested by Author(s))

Structures
Composites

Date for general release August 1992

Subject Category 15

19. Security Classif. (of this report)	20. Security Classif. (of this page)	21. No. of pages	22. Price
Unclassified	Unclassified	35	

NASA FORM 1626 OCT 86

formati

NASA-Langley, 1990